



8-2006

A Quantitative Study of Scaling Properties of Fracture Networks

Ankur Roy
University of Tennessee - Knoxville

Follow this and additional works at: https://trace.tennessee.edu/utk_gradthes



Recommended Citation

Roy, Ankur, "A Quantitative Study of Scaling Properties of Fracture Networks. " Master's Thesis, University of Tennessee, 2006.
https://trace.tennessee.edu/utk_gradthes/1780

This Thesis is brought to you for free and open access by the Graduate School at TRACE: Tennessee Research and Creative Exchange. It has been accepted for inclusion in Masters Theses by an authorized administrator of TRACE: Tennessee Research and Creative Exchange. For more information, please contact trace@utk.edu.

To the Graduate Council:

I am submitting herewith a thesis written by Ankur Roy entitled "A Quantitative Study of Scaling Properties of Fracture Networks." I have examined the final electronic copy of this thesis for form and content and recommend that it be accepted in partial fulfillment of the requirements for the degree of Master of Science, with a major in Geology.

Edmund Perfect, Major Professor

We have read this thesis and recommend its acceptance:

William M. Dunne, Larry D. McKay

Accepted for the Council:

Carolyn R. Hodges

Vice Provost and Dean of the Graduate School

(Original signatures are on file with official student records.)

To the Graduate Council:

I am submitting herewith a thesis written by Ankur Roy entitled “A Quantitative Study of Scaling Properties of Fracture Networks”. I have examined the final electronic copy of this thesis for form and content and recommend that it be accepted in partial fulfillment of the requirements for the degree of Master of Science, with a major in Geology.

Edmund Perfect

Major Professor

We have read this thesis
and recommend its acceptance:

William M. Dunne

Larry D. McKay

Accepted for the Council:

Anne Mayhew

Vice Chancellor and Dean of Graduate Studies

(Original signatures are on file with official student records)

A Quantitative Study of Scaling Properties of Fracture Networks

A Thesis Presented for the
Master of Science Degree
The University of Tennessee, Knoxville

Ankur Roy

August, 2006

ABSTRACT

Fracture networks and their scaling properties are important from both an academic and practical perspective since they play a significant role in many areas ranging from crustal fluid flow to studies of earthquakes. Over the years, researchers have employed a wide variety of techniques to quantify the complexities of fractured media. These range from deterministic, process-based approaches employing the laws of physics, to ones involving the applications of geostatistics and more recently, fractal geometry. Fractals are irregular entities that show self-similarity over a wide range of scales and can be quantified by the fractal dimension, D . It is important that the D -values of such networks are properly evaluated. The box-counting algorithm is a widely used technique for characterizing fracture networks as fractals and estimating their D -values. If this analysis yields a power law distribution given by $N \propto r^{-D}$, where N is the number of boxes containing one or more fractures and r is the box size, the network is considered to be fractal. However, researchers are divided in their opinion about issues such as the best box-counting algorithm for estimating the ‘correct’ D -value or whether a fracture network is indeed fractal. For instance, a closer look at the N vs. r plots for a set of previously published fracture trace maps shows that such distributions do not follow power law scaling. As part of the present work, a synthetic fractal-fracture network with a known theoretical fractal dimension, D , was used to develop an improved algorithm for the box-counting method that returns “unbiased” D -values. A suite of 17 fracture trace maps that had previously been evaluated for their fractal nature was reanalyzed using the improved technique. “Unbiased” estimates of D for these maps ranged from 1.56 ± 0.02 to 1.79 ± 0.02 , and were much higher than the original estimates. The fractal dimension of a pattern however, does not capture all of the heterogeneity present. For instance, two patterns that have the same fractal dimension may have very different appearances. We investigated the applicability of a new parameter, namely lacunarity, L , for distinguishing between different fracture networks having the same fractal dimension. The lacunarity is the degree of clustering in a pattern and is a geostatistical parameter that can be used to study patterns that are both fractals non-fractal. The gliding-box algorithm is a popular

technique for computing lacunarities as a function of the box-size, r . In the present work it has been successfully used for the first time to analyze fracture networks. Apart from computing lacunarity curves for a set of synthetic patterns generated in MATLAB, we also analyzed a set of 7 nested natural fracture maps with similar D values ranging from 1.80 ± 0.05 to 1.84 ± 0.04 . Our results show that differences between maps are most pronounced when L values are determined using intermediate box sizes. Estimates of L based on such box sizes indicate that fractures are more clustered at smaller scales. Future work in this area should explore the use of the gliding box algorithm to see whether fracture networks are self-similar over a given range of scales and if lacunarity analysis alone can furnish information on the “unbiased” fractal dimensions of such networks.

Table of Contents

Section	Page
Introduction	1
PART I	
Fractal Characterization of Fracture Networks: An Improved Technique	4
1. Introduction	5
2. Theory	8
2.1 Fractals and the Fractal Dimension	
2.2 Synthetic Fractal-Fracture Pattern	
2.3 Analytical Box-counting on Fractal-Fracture Patterns	
3. Modified Box-counting Algorithm	13
4. Application to Fracture Networks	17
4.1 Synthetic Fractal-Fracture Networks	
4.2 Analysis of Natural Patterns in Nested Maps	
4.3 Analysis of Individual Maps	
5. Conclusions	24
References	27
Appendices IA-IC	30
PART II	
Lacunarity Analysis of Fracture Networks	45
1. Introduction	46
2. Synthetic Fractal-Fracture Patterns	49
3. Theory	52
2.1 Translational Invariance	
2.2 Lacunarity	
2.3 The Gliding-box Algorithm	
4. Data Analysis and Results	56
4.1 Synthetic Fracture Networks	
4.2 Natural Fracture Networks	
5. Discussion and Conclusions	60
References	63
Appendices IIA-IIF	65
GENERAL APPENDICES	
Appendices A-B: maps used	81
Vita	103

List of Tables

No.	page
1.1 Percentage errors in evaluating D_b for synthetic patterns using whole range of data points and points turned off for $r < proxy\ r_{min}$ and $r < r_{min}$	33
1.2 Odling's (1997) maps: scales, $proxy\ r_{min}$ (in meters), modified box-counting dimension D_b and capacity dimension D^* (Bour et al., 2002)	33
1.3 Barton's (1995) maps: reported l_{min} , $proxy\ r_{min}$ (in meters) for uncropped maps, $proxy\ r_{min}$ for cropped maps, D_b evaluated by Barton (1995), D_b evaluated using whole range of data points, D_b (fractal dimension from uncropped maps) and $(D_b)_c$ (fractal dimension from cropped maps)	34
2.1 Fracture porosities and lacunarities, $L\ (31)$ and $L\ (450)$, of synthetic fractal-fracture patterns with $D = 1.585$	71
2.2 Odling's (1997) maps: scales, $proxy\ r_{min}$ (in meters), fractal dimension D_b , fracture porosity and lacunarities L_{upper} , $L\ (10)$ and $L\ (500)$	71

List of Figures

No.		page
1.1	Construction of a deterministic Sierpinski lattice with $b=2$ and $n=1$: (a) basic template $i = 0$ with two fractures of length 1, (b) $i = 1$: addition of fractures of length $1/2$, (c) $i = 2$: addition of fractures of length $1/4$, (d) $i = 3$: addition of fractures of length $1/8$, (e) $i = 4$: addition of fractures of length $1/16$ (f) $i = 5$: addition of fractures of length $1/32$	36
1.2	Analytical box-counting showing N (no. of boxes) vs. r (box-size) plots for fractures in synthetic pattern with $b=2$, $n=1$ and $i=20$	37
1.3	Plot showing N (no of boxes) vs. r (box size) for synthetic pattern with $b=2$, $n=1$, $i=4$ with whole range of data points and those for which $r < r_{min}$, “turned off”	38
1.4	Plot showing variation of D_b with i for synthetic pattern $b=2$, $n=1$: D_b ($\pm 95\%$ confidence intervals) computed using whole range of box-sizes, box-sizes larger than the r_{min} and box-sizes larger than the <i>proxy</i> r_{min}	39
1.5	Plot showing $d(SD)/dr$ vs. r for synthetic pattern $i = 4$ used for finding the <i>proxy</i> r_{min} (theoretical $r_{min} = 63.23$)	40
1.6	Plot showing relationship between r_{min} and <i>proxy</i> r_{min} for synthetic pattern with $b = 2$, $n = 1$ at different iteration levels ($i = 1 - 6$)	41
1.7	$N_{adjusted}$ vs. r_m for maps 1-7 from Odling (1997)	42
1.8	Plot showing relationship between l_{min} and <i>proxy</i> r_{min} for Barton’s (1995) maps	43
1.9	Comparison of fractal dimensions of Barton’s (1995) maps as computed by Barton (1995), Berkowitz and Hadad (1997) and using the improved method	44
2.1	Construction of the deterministic fractal-fracture model b2n1_det: (a) basic template $i = 0$ with two fractures of length 1, (b) $i = 1$: addition of fractures of length $1/2$, (c) $i = 2$: addition of fractures of length $1/4$, (d) $i = 3$: addition of fractures of length $1/8$, (e) $i = 4$ (b2n1i4_det): addition of fractures of length $1/16$, (f) randomized version of (e) (b2n1i4_ran)	73

No.	List of Figures (continued)	Page
2.2	Deterministic (a) and randomized (b) fractal-fracture patterns (b4n7i2_det and b4n7i2_ran, respectively)	74
2.3	Translationally invariant set: simple 32 X 32 grid (non-fractal)	75
2.4	Linear patterns showing same number of filled units but differing in spatial distribution (from Turcotte, 1997)	75
2.5	Gliding window algorithm showing distribution of $n(s, r)$ for $r=9$ (from Turcotte, 1997)	76
2.6	Lacunarity analyses of the distributions shown in 2.4 (from Turcotte, 1997)	76
2.7	Gliding-window in a typical fracture pattern: b2n1i4_det	77
2.8	$L(r)$ vs. r plots for patterns b2n1i4_det, b2n1i4_ran, b4n7i2_det, b4n7i2_ran and trans-inv	78
2.9	Mean and standard deviations of $L(r)$ vs. r plots for 10 randomized versions of b2n1i4_ran	78
2.10	$L(r)$ vs. r curves for Odling's maps 1-7	79
2.11	$L_{upper} (=1/\phi)$ vs. $L(10)$ for Odling's maps 1-7	80

INTRODUCTION

Fractures are developed by brittle failure and are defined as discrete breaks within a rock mass across which cohesion is lost. They include both faults with in-plane shear and joints with opening mode behavior. Open fractures allow rapid transport of fluids and contaminants through rock masses. Since the mid-nineteen eighties interest in the hydrological and geo-mechanical properties of fractured rock has gained appreciable momentum in the scientific community. However, modeling and prediction of flow through fractured media remains a challenging task.

Fractures exist over a wide range of scales from microns (in thin sections) to hundreds of kilometers (as in transform faults). Their size scaling and spatial clustering attributes are important for understanding fractured rock hydrology and bulk mechanical properties. Fracture patterns tend to become more complex in nature as fractures are superimposed during two or more deformational episodes. The importance of fractures and their scaling characteristics lies in applied areas such as modeling of flow through fractured aquifers and along fractures in the interwell volume of petroleum reservoirs, where fractures on scales that are significant to flow are not represented in either seismic reflections or well logs. Another application includes the study of faults in relation to the prediction of earthquakes.

Various attributes of fracture networks have been quantified. Most of the approaches have been statistical in nature such as studies about the distribution of orientation, length scaling, aperture size distribution etc. Some approaches on the other hand have looked at fracture patterns as a whole using the concepts of fractal geometry, thus incorporating the distributions of length, barycentres and orientation into a single analysis. In a nutshell, fractals are entities that display self-similarity over a wide range of scales, which means that any proportion of such a pattern is a scaled down version of the whole. The very fact that fractures exist over a wide range of scales makes them interesting from the perspective of fractal geometry.

Over the past few years discussion has centered on the issue of whether fracture networks can be characterized as fractals and if a single fractal parameter can completely describe such a pattern. In this study, a two-step approach was taken. The first part deals with addressing the question of whether fractal geometry can be successfully used to harness the complexities of natural fracture networks. The second part goes a step further and addresses the issue of whether fracture networks can be satisfactorily quantified using a more generalized approach based on lacunarity. In this case, researchers need not begin with any preconceived notion on whether or not a fracture network is fractal. The entire study involves a modeling component and analysis of synthetic (fractal) as well as natural fracture networks.

PART I

Fractal Characterization of Fracture Networks: An Improved Technique

1. INTRODUCTION

Fracture systems have been a focus of research for decades owing to their importance in a variety of fields including fluid flow in the earth's crust, contaminant transport, engineering geology and seismology. Joints and faults are two primary types of fractures. Joints are mode I fractures where displacement is *normal* to the propagating fracture walls (opening mode). Faults are mode II fractures, where displacement is parallel to the walls of the discontinuity (in-plane shear mode). Fractures exist over a wide range of scales – from microns (in thin sections) to thousands of kilometers (as with plate-bounding faults) and typically develop more complex patterns in a region as fracturing events are superimposed through time. These characteristics potentially make them interesting from the perspective of fractal geometry. Fractals are entities displaying self-similarity over a wide range of scales, which means that any portion of a fractal entity is a scaled down version of the whole (Mandelbrot, 1983). Such patterns can be quantified by a parameter, namely the fractal dimension, which is related to the way in which the complexities of the network fill up the embedding Euclidean space.

The earliest attempt to identify fractal characteristics in fractures is documented in Barton and Larsen (1985) where the box-counting method was used by manually placing grids of various sizes over maps of three different rock pavements in welded tuff, and counting the number of grid elements, N , intersected by the fracture traces. Ever since, many workers have attempted to analyze fracture patterns using various modifications of this method [Chiles, 1988; La Pointe, 1988; Gillespie et al., 1993; Walsh and Watterson, 1993; Barton, 1995; Ouillon et al., 1996; Berkowitz and Hadad, 1997; Babadagli, 2000]. Others have attempted to find fractal characteristics in the distributions of fracture lengths or apertures [Odling, 1997; Odling, 1999; Marrett et al., 1999; Bour et al., 2002]. Details on most of these works with critiques on the methods used can be found in the review paper by Bonnett et al. (2001). However, in spite of the large number of investigations, researchers are still divided as to whether fracture networks can be characterized as fractals at all. Also, since different workers have reported different values of the fractal dimension for the same map, a technique for evaluating the fractal dimension that has wide acceptance and can be used for future research remains to be developed.

Notwithstanding the fact that fracture networks have not been unequivocally established to be fractal in nature, and that the value of the fractal dimension varies with the method employed, workers have tried to relate this parameter to physical processes such as flow and transport (Doughty and Karasaki, 2000) and the percolation threshold (Zhang and Sanderson, 1994). Others like Zhang and Zhou (2000) list research endeavors that seem interesting in light of the fact that normal, reverse and strike-slip faults were said to have high, medium and low fractal dimensions respectively. Therefore, establishing whether fracture networks are fractals is still important. If the answer is yes, we need to have a technique for computing “unbiased” fractal dimensions of such networks.

Our present research is therefore an endeavor to address these questions by developing with a modified version of the box-counting method. The method that we describe has been tested on a model with a known theoretical fractal dimension and on a nested set of 7 fracture patterns (Odling, 1997). If our method returns a consistent value for the fractal dimension for each of these maps it may be proved that a more detailed map from a smaller section of the whole region is essentially a scaled down version of the latter. Finally we have examined a set of 17 fracture maps previously published and analyzed by Barton (1995) and later reanalyzed by Berkowitz and Hadad (1997) and attempted to address discrepancies in the results between different estimates of the fractal dimension.

2. THEORY

We constructed a fractal-fracture pattern following Samis et al. (1986) and tested our new method on this synthetic pattern before examining natural fracture networks. In this section, we briefly introduce the concept of a fractal and the fractal dimension before developing our model. We also use this synthetic pattern to demonstrate that an analytical box-counting algorithm returns an exact value for the theoretical fractal dimension.

2.1 Fractals and the Fractal Dimension

Fractals are entities that display self-similarity in their geometry such that any portion of the system is a replica of it as seen at a larger scale. In simplistic terms, the fractal dimension describes the manner in which a fractal entity fills up the Euclidean space. More precisely, Mandelbrot (1983) defines a fractal as a set for which the Hausdroff Besicovitch dimension (D) strictly exceeds the topological dimension. Therefore, every set with a non-integer D is a fractal but it is not necessary that all fractal dimensions be non-integers. For most of our purposes we will be dealing with non-integer fractal dimensions.

The most popular approach for determining fractal dimensions of fracture maps is the box-counting technique. Basically, it involves overlaying the map with a sequence of grids, each with a different cell size, r and counting the number of occupied cells, N . The fractal dimension, referred to as D hereafter, is simply the slope of a plot of $\log N$ vs. $\log r$. We will return to the details of its estimation in a later section. Structural geologists have preferred to report the fractal dimension of fault trace length distributions for the slope of the plot of the \log (size) vs. the \log (cumulative number). In our model, however, we show that simply using the number of fractures (N_f) instead of the cumulative number provides the exact fractal dimension.

2.2 Synthetic Fractal-Fracture Pattern

A fractal-fracture pattern is constructed using hierarchical fracture networks composed of line segments in 2D. The networks are essentially generated as deterministic Sierpinski lattices. Three basic parameters are used for generating the patterns – scaling factor: b , number of blocks not iterated at each step: n and iteration: i . A value of $b = 2$ is used such that the initial square template consists of two orthogonal fractures dividing the whole area into four blocks each with a side of length 0.5 (Fig 1.1a; all tables and figures in appendices I B-C). We call this the initiator such that $i=0$. In the next step, one block is left unfractured and the others are reiterated by shrinking this template ($i=0$) by a factor of 2, replicating it $b^2 - n = 2^2 - 1 = 3$ times and finally superimposing the replicated traces on the original template thus creating the generator, $i=1$ (Fig 1.1b). This generator is then applied onto itself in successive iterations until $i=6$, thus creating a sequence of 7 patterns for $i=0$ to 6 (Fig 1.1a-f). Doughty and Karasaki (2002) also used a similar model with $b=3$ and $n=1$ to 8 for simulating flow through hierarchically fractured rocks.

The theoretical fractal dimension, D of the patterns generated is the same for all i and may be found from equation (1) as follows:

$$D = \frac{\log(b^2 - n)}{\log b} \dots\dots\dots(1)$$

In Fig 1.1:

$$D = \frac{\log(2^2 - 1)}{\log 2} = \frac{\log 3}{\log 2} = 1.585$$

The length distribution of the fractures in this pattern can be found from the equations

$$N_f = 2(b-1)(b^2 - n)^i \dots\dots\dots(2)$$

$$l = 1/b^i \dots\dots\dots(3)$$

where, N_f is the number of fractures of length l at an iteration level of i . It needs to be emphasized that equations (1) to (3) hold good for any set of b and n values. In our

particular case $b=2$, $n=1$. Also note that since D is independent of i , all patterns we have generated have, at least theoretically, the same fractal dimension.

Here, we show analytically that the length count approach yields the same D -value as given by equation (1). Taking the logarithm on both sides, equations (2) and (3) can be rewritten as:

$$\log(N_f) = \log 2 + \log(b-1) + i \log(b^2 - n) \dots\dots\dots(4)$$

$$\log(l) = -i \log b \dots\dots\dots(5)$$

rewriting equations (4) and (5) in derivative form:

$$d \log(N_f) = [\log(b^2 - n)] di \dots\dots\dots(6)$$

$$d \log(l) = -[\log(b)] di \dots\dots\dots(7)$$

dividing (6) by (7) we can eliminate di between the two and obtain the slope of the line for a log (size) vs. log (number) plot as:

$$\frac{d \log(N_f)}{d \log(l)} = -\frac{\log(b^2 - n)}{\log b} \dots\dots\dots(8)$$

substituting equation (1) into equation (8) yields:

$$\frac{d \log(N_f)}{d \log(l)} = -D \dots\dots\dots(9)$$

For this model, it can also be shown analytically that the more popular cumulative length count approach yields the fractal dimension only as i tends to infinity (Appendix A).

2.3 Analytical Box-counting on Fractal-Fracture Patterns

Before the synthetic patterns were empirically box-counted for estimating the D , a set of analytical expressions for a general b and n is developed for a better understanding of our pattern. We begin by constructing our model with parameters b and n . We then overlay

smaller and smaller grids of size, r such that the scaling factor of the box-sizes, β is the *same* as the scaling factor of the underlying lattice of the model, b i.e.:

$$r = \beta^{-i} = b^{-i} \dots\dots\dots(10)$$

In our particular case of $b=2$, $n=1$, the boxes scale as 1, 1/2, 1/4, 1/8 etc and the minimum grid size, $r_{min} = l_{min} = 1/b^{imax}$, where $imax$ is the maximum iteration level and l_{min} is the *smallest* fracture length in a particular pattern. Note that this is also the smallest fractal element in the pattern.

For a fractal pattern, the number of occupied boxes, $N_{occupied}$ is given as:

$$N_{occupied} = r^{-D_b} \dots\dots\dots(11)$$

where, D_b is the fractal dimension

Equation (11) when plotted for $b=2$, $n=1$ and $i=20$, yields a straight line (Fig 1.2). This analytical box-counting exercise clearly demonstrates that the synthetic fractures are fractal. To further note, this analytical model can test the fractal nature of any pattern with varying values of b and n .

3. MODIFIED BOX-COUNTING ALGORITHM

The commercially available Benoit software (www.trusoft-international.com) allows for box-counting such that the pattern of interest can be overlaid by square grids of different sizes that can be rotated to find the minimum number of occupied boxes for a particular size. Use of the minimum number of occupied boxes is invoked here so as to accommodate a boundary condition stated in the derivation of equation (11) by Hausdroff (1919). The software generates an array of points for N (number of occupied boxes) vs. r (box-size) on a log-log scale and fits a line to it, the slope of which gives the box-counting fractal dimension, D_b of the pattern. One can manually “turn off” points on the plot so that the regression line is fitted to a subset of the whole range of data set at the user’s discretion. For our purpose, the side length of the largest box is fixed at 1/2 the width or length of the map, whichever is smaller. The scaling factor of the box sizes, β is the factor by which the box-sizes are divided during the progression from the largest to the smallest box size, the progression always being geometric (i.e. for $\beta = 2$, box-sizes are 16, 8, 4, 2, 1). For our empirical box-counting we set $\beta = 1.1$ (as opposed to 2 in our analytical box-counting discussed earlier) so that the number of box sizes (data points) is maximized in each case, thus generating a robust data set. The number of data points, P is given by the following equation: $P = \log (\text{side length of largest box}) / \log \beta$. The increment of grid rotation is set to 1° and the grid is rotated by a full 90° such that the algorithm determines the smallest number of occupied boxes from an array of 90 ($= 90/1$) data points for each box size.

The six synthetic patterns ($i = 0 - 5$) that we created were box-counted in the Benoit platform and it was found that none of these patterns yielded points that fell on a straight line (e.g., Fig 1.3). Walsh and Watterson (1993) and Gillespie et al (1993) have also reported the curved nature of data plots from box-counting. A closer examination of similar plots published by Barton (1995) for his set of 17 maps show that they do not really fall on straight lines. Figure 6, depicting the fractal dimension of fractured rocks, in the work of Zhang and Sanderson (1994) also reveals the same artifact. The curvature observed raises questions about the fractal nature of these fracture patterns. It is further noted that quite contrary to theoretical ideas discussed earlier, for our model the D_b -value

systematically increases with the iteration level, i if the whole range of values is considered (Fig 1.4)

In the box-counting algorithm, when the box-size r becomes smaller than the smallest fractal-fracture element present, no new elements are revealed and counted. As a result the N (number of occupied boxes) vs. r (box-size) relationship on the log-log scale deviates from its theoretical straight-line behavior and becomes curvilinear. Therefore, fitting a straight line to the entire range of data points returns a spurious fractal dimension and may further give the impression that the pattern under investigation is not a true fractal. However, a straight line, the slope of which gives the true fractal dimension of the pattern, should only be fitted to those data points for which the r is larger than (or equal to) a limiting value r_{min} . For our analytical box-counting discussed earlier, where the scaling factor of the box-sizes, β is same as the scaling factor of the underlying lattice of the model, i.e. $\beta = b = 2$ in our case, the boxes scale as 1, 1/2, 1/4, 1/8 etc and $r_{min} = l_{min} = 1/b^{imax}$, where $imax$ is the maximum iteration level and l_{min} is the smallest fracture length in a particular pattern. This is also the smallest element in the fractal pattern. However, in the case of empirical box-counting for the same model, β was chosen to be 1.1 so that a more robust set of data points would be generated. As a result the limiting box-size at which all the boxes appear unfilled is *larger* than the value $r_{min} = 1/b^{imax+1}$ by an infinitesimally small amount. This means that for a pattern of $i=5$, $l_{min} = 1/2^5 = 0.312$ and $r_{min} \rightarrow 1/2^6$. Accordingly, points for which $r < r_{min}$ are easily “turned off” in the plot (Fig 1.3), thereby yielding a better estimate of the true fractal dimension.

Although r_{min} is known for our synthetic fractal-fracture networks, it is unknown for natural patterns. Therefore, a method for estimating a proxy value for r_{min} needs to be determined. For each pattern the standard deviation, SD , from the regression equation for the line of best fit in the N vs. r plot, is noted in a systematic manner for points “turned off” at increasing r -values. The idea is to attain an r -value for which the incremental change in the SD of the best-fit line is minimized. In order to achieve this, the $d(SD)/dr$ is calculated to find the r -value at which the slope of the SD goes to zero. However, in some

cases, because of statistical fluctuations in the data points, the $d(SD)/dr$ function jumps back to a small non-zero value after initially reaching zero. Therefore, in order to find the best estimate for the r_{min} value (i.e. the one nearest to the theoretical r_{min}) we employed the condition that the $d(SD)/dr$ function remain at zero for at least three consecutive r -values (Fig 1.5). This value is the *proxy* r_{min} and all points for which $r < \text{proxy } r_{min}$ are then excluded from fitting the straight line. This algorithm is used on our synthetic patterns to test how good an estimate of the D_b -value it provides when used instead of the theoretical r_{min} value for “turning off” the points on the N vs. r plots. Although the *proxy* r_{min} consistently underestimates the theoretical r_{min} values (Fig 1.6) its use nonetheless returns very good estimates of the D_b as compared to those obtained by fitting over the whole range of r values (see next section).

4. APPLICATION TO FRACTURE NETWORKS

4.1 Synthetic Fractal-Fracture Networks

The variation of D_b 's estimated considering the whole range of data points, and following truncation based on the r_{min} and the *proxy* r_{min} values, with i , is shown in Fig.1.4. From the plot it can be seen that D_b computed using the whole range of r values increases with increasing i , while consistently underestimating the theoretical D -value. The error bars around the D_b -values are small and are consistent over whole range of i ; this is because the same number of data points was used in the best fits regardless of the iteration level. On the other hand, the D_b 's obtained by not considering the r -values smaller than the r_{min} and the *proxy* r_{min} respectively, stabilize at $i = 3$ and approximate the theoretical D -value of 1.585. The error bars around the D_b -values become smaller with increasing i . This happens because the number of points used for calculating the slope of best fit increases with the iteration level; i.e. the error associated with the estimates increases as the r_{min} and *proxy* r_{min} values increase. The D_b -values determined using the r_{min} and the *proxy* r_{min} truncation points are nearly identical for $i \geq 3$ (Fig 1.4). However, they do result in a slight overestimate of the theoretical value. For $i \geq 3$ the magnitude of this bias is very small compared to the systematic bias introduced by fitting over the whole range (Table 1.1). In general, these results imply that using *proxy* r_{min} in place of the r_{min} does not influence box-counting estimates of the theoretical D value. The idea is further supported by Fig 1.6 which shows that there exists a good correlation between the r_{min} and the *proxy* r_{min} determined for all the patterns from $i = 1$ through 6. Also, table 1.1 shows that using the *proxy* r_{min} , the D values for $i > 2$ can be evaluated within an error of 3.5%. Therefore the *proxy* r_{min} may be used instead of the r_{min} for evaluating the box-counting fractal dimension, D_b in the case of natural fractures where a value for the latter is not normally available.

The above results are promising from the perspective of natural networks where fracture lengths commonly range over one or two orders of magnitude (Barton, 1995). This size range is important because starting at $i = 4$, the lengths of our synthetic fractures are distributed over two orders of magnitude since $l_{min} = 1/b^i = 1/2^4 = 0.0625$ and $l_{max} = 1$.

Therefore, this method should work well in case of natural fractures since they have the same relative length ranges as the synthetic pattern.

4.2 Analysis of Natural Patterns in Nested Maps

Having established a synthetic fracture pattern with a known fractal geometry, we also identified natural fracture patterns for testing our modified box-counting approach. One natural data set is suite of 7 nested fracture patterns mapped in the same area of Hornelen basin, Norway (Appendix A) by Odling (1997). Each map is a subset of the larger area (Figure 1 in Bour et al., 2002) and is mapped from a lower elevation such that it represents a limited scale range of joint trace lengths controlled by the image resolution. The original 7 maps, received as encapsulated postscript files from Dr Odling, were converted into bitmap images at 500dpi resolution using Adobe Illustrator. If the 720m x 720m pattern is self-similar, all maps should have the same fractal dimension because one is essentially a scaled down version of the other. These maps were also used by Bour et al (2002) to compute capacity dimensions and in our work we present a comparison between these values (Table 1.2)

The *proxy* r_{min} and the fractal dimension are two parameters that were evaluated for this data set. The former changes systematically with the scale suggesting that it responds to the smallest fracture length present at each scale and can thus be considered an estimate for the minimum observed fracture length at a given scale and resolution. It may be noted here that given the fact that map 4 was photographed from a higher elevation than map 3 it is expected that the latter should yield a smaller *proxy* r_{min} (meter). However, since a higher resolution camera (Hasselbald) was used in case of map 4 as compared to map 3, this change compensated for the height effect (personal communication with Noelle Odling, March 06, 2006).

The box-counting fractal dimension D_b , varies from 1.80 ± 0.05 to 1.84 ± 0.04 (Table 1.2). Comparing with the capacity dimension, which is equivalent to the box-counting fractal

dimension, determined by Bour et al (2002), D_b lies within a narrower range and exhibits less variation in terms of the 95% confidence limits. It may therefore be said that the D value remains almost constant throughout the different scales. Not only does this further support the fact that the 720m x 720m pattern is a fractal but also that our method returns an “improved” box-counting D_b value.

Further, the N vs. r data from all 7 maps were converted to meter scaling and plotted on a single graph (Fig 1.7). The r_{pix} value, (i.e. r in terms of pixels) was converted to r_m using $r_m = r_{pix} \times (\text{side length of map area in m})/(3473)$, where 3473 is the length of the map area in pixels. The N value was accordingly adjusted using: $N_{adjusted} = N \times [720/(\text{side length of map area in m})]^{1.82}$, where 720 is the side length of the largest map (in meters) and 1.82 is the average fractal dimension computed by averaging the D_b values in table 1.2. The points from all the maps encompass a scale range of more than 3 orders of magnitude. This shows in a very convincing manner that the Hornelen basin fracture pattern is a fractal over at least 3 orders of magnitude.

4.3 Analysis of Individual Maps

Given that our modified box-counting approach that only considers box-sizes larger than a particular *proxy* r_{min} value yields an “improved” fractal dimension we analyzed a series of 17 previously published fracture trace maps from a variety of tectonic settings, lithologies and scales (Barton, 1995). All maps were scanned at 500dpi in B/W line-mode using a standard scanner into Photoshop. Two sets of maps were created from the scanned images (Appendix B). The first map set was made by rotating the images and drawing a rectangle around them so as to exclude any “unmapped” white areas while including all of the fractures such that there is no loss of data. The other set was created by rotating the images and cropping them by drawing the largest possible rectangle within a pattern such that it would capture the maximum subset of the entire data without any “unmapped” white areas. However, maps i, m and p were not included in this second set because they did not have any “unmapped” white areas. A different set of cropped

versions of these maps was analyzed by Berkowitz and Hadad (1997) who reported higher D -values. In our work, we compared the D 's and endeavored to explain their differences thereof.

A plot of the *proxy* r_{min} values for the uncropped maps versus the minimum lengths (l_{min}) as reported by Barton shows two important characteristics (Fig 1.8). First it displays the scale range of the maps – from microscopic (map q) to that of transform faults (map p) of over eight orders of length magnitude. Secondly, it shows that the *proxy* r_{min} is well correlated with the l_{min} parameter (coefficient of determination, $R^2 = 0.961$) such that former is a very good estimate of the latter. When the second set of cropped maps was used for determining *proxy* r_{min} the values returned were very close (exactly the same in cases of maps c and g) although consistently higher in most cases with the exception of map a (table 1.3).

The second set of maps was created by cropping 14 of 17 maps as described earlier to investigate whether, in the case of maps with irregular boundaries, it is appropriate to crop maps before evaluating their fractal dimensions. One clear advantage is that cropping eliminates all white areas containing “no data”. At the same time it is important to consider that the cropped area should be representative of the entire region. An example of this issue is maps without white areas may not be representative of the pavement, because they are more fractured than average across the region (personal communication Randall Marrett, March 21, 2006). Thus in some cases, the white areas without fractures may really be part of the data set. Also, another problem is that cropping can eliminate the smallest fracture from the pattern and overestimate the *proxy* r_{min} value (table 1.3). So, the use of cropping is a trade off between analyzing a pattern with the complete data (all fractures included) and a pattern with a few missing fractures but no “unmapped zones” which might also bias the D value. Our results, show that cropping might not be that serious an issue because for each of the maps analyzed the fractal dimensions computed from the cropped maps, $(D_b)_c$ fell within the same range as those computed from the uncropped ones denoted by D_b in table 1.3. The two sets of

estimates yielded a coefficient of correlation of $r = 0.89$. For all purposes of comparing our results with those of others we have used the D_b 's obtained from the un-cropped versions.

Comparing D_b values evaluated using the modified box-counting method with those of Barton's (1995) and Berkowitz and Hadad's (1997), the former are underestimates while the latter are overestimates (Fig 1.9). It can be seen from table 1.3 that our box-counting results without "turning off" the data points for which $r < \text{proxy } r_{min}$ i.e. considering the whole range of data points, returned consistently lower estimates of the true fractal dimension and that the values were very similar to those reported by Barton (1995). In fact, for maps d, f and m the values are exactly the same. This shows that if the data points for which $r < \text{proxy } r_{min}$ are considered for fitting the straight line to the plot we end up with spurious D_b -values even though the R^2 may be high.

The dimensions reported by Berkowitz and Hadad (1997) on the other hand are over estimates of the "unbiased" fractal dimension. One of the reasons cited by the authors for values higher than Barton's is that cropping the maps to remove "arbitrary boundaries" increased the fractal dimension. Clearly this is not the case since a comparison of the values estimated by our method from cropped and un-cropped maps (table 1.3) show that they fall within the same range of each other and are consistently lower than all the values reported by Berkowitz and Hadad (1997).

However, the question still remains as to the differences between our results and those of Berkowitz and Hadad (1997). We suggest that they may be related to differences in the map resolution and/or the scaling factor, β , employed in the two studies. For instance, one of their digitized maps (map b) was only 128×128 pixels, whereas ours was 2063×1463 . The lower resolution employed by Berkowitz and Hadad may have yielded inaccurate box counts for the smallest box sizes. Furthermore, the larger the β value, the fewer the number of points on the box-counting curve. Their plot for map b has only 5 data points whereas in our modified box-counting plot there were 28. This is because the

scaling factor of the box-sizes was $\beta = 2$ in their analyses as opposed to $\beta = 1.1$ in ours. The importance of a robust the data set cannot be overemphasized since the use of a just few points to fit a straight line has already met with criticism and raised doubts about the fractal nature of the fracture network under investigation (e.g., Bonnet et al, 2001).

5. CONCLUSIONS

Our synthetic fractal-fracture pattern, which is a generalized version of Sammis' (1986) model, is a powerful one that helps prove a number of points. First of all it demonstrates that the length count approach returns a good value for the theoretical fractal dimension of a pattern just as the box-counting approach does. It also illustrates the fact that if the points on the $\log N$ (occupied boxes) vs. $\log r$ (box-size) plot, for which $r < l_{min}$ are “turned off” the resulting array of points can be fitted by a straight line whose slope gives the true fractal dimension of the pattern. Finally it helps in realizing the *proxy* r_{min} parameter and proves that it is a fair estimate of the minimum fracture length in the pattern.

Our analyses of Odling's maps from the Hornelen basin in Norway proves that fracture patterns can indeed be fractals and repeat themselves over at least 3 orders of magnitude. The results from this analysis coupled with those from our model also helped us demonstrate that our modified box-counting technique is a novel one that can be used with any other fracture pattern to check for fractal characteristics and evaluate their fractal dimension.

We further analyzed a series of 17 previously published fracture trace maps from a variety of tectonic settings, lithologies and scales (Barton, 1995). All of these maps have been previously analyzed for their fractal dimension (Barton, 1995; Berkowitz and Hadad, 1997). The analyses of these maps returned two parameters: *proxy* r_{min} and D_b . The former proved to be excellent estimates of the measured minimum length values (Barton 1995). The latter, however, was found to be very different from the values reported both by Barton (1995) and Berkowitz and Hadad (1997). For each of the 17 maps analyzed, the “improved” D_b value was consistently higher than that of Barton's (1995) and lower than that of Berkowitz and Hadad's (1997). The modification in the box-counting algorithm employed by us is the reason for the difference between our results and those of Barton's (1995). On the other hand, the difference in the map resolution appeared to be the main reason for our values being different from those of Berkowitz and Hadad (1997). The maps were also cropped and reanalyzed to see the

effects of cropping on the algorithm. It was seen that although the D_b and $(D_b)_c$ values did differ, in most cases they fell within an acceptable range of each other and so the cropped sections were considered representative of the entire network.

In conclusion, it may be said that although many workers have argued over the fractal nature of fractures, some networks (at least those discussed here) can be truly self similar such that their geometries can be described by a single parameter, namely the fractal dimension. However, whether the D_b value can be related to any geomechanical properties of the rock or the stress regime that generated the fractures remains to be addressed. Also, it should be noted that fracture networks that look different from each other might have the same fractal dimension and it needs to be investigated whether any other parameter, apart from the D_b value, can be used for characterizing a particular pattern uniquely.

REFERENCES

- Babadagli, T., 2000, Evaluation of outcrop fracture patterns of Geothermal reservoirs in Southwestern Turkey, *Proceedings World Geothermal Congress 2000, Japan*, 2,521-526
- Barton, C. C. and Larsen, E., 1985, Fractal Geometry of two-dimensional fracture networks at Yucca Mountain, Southwestern Nevada, *Proceedings of the International Symposium on fundamentals of Rock Joints*, 77-84
- Barton, C. C., 1995, Fractal analysis of scaling and spatial clustering of Fractures, in Barton C. C., and La Pointe, P., eds., *Fractals in the Earth Sciences*, Plenum, NewYork, 265pp.
- Berkowitz B., Hadad, A., 1997, Fractal and multifractal measures of natural and synthetic fracture networks, *Journal of Geophysical Research*, vol. 102, no. B6, 12,205-12,218.
- Bonnet E., Bour, O., Odling, N. E., Davy, P., Main, I., Cowie, P., Berkowitz, B, 2001, Scaling of fracture systems in Geological Media, *Reviews in Geophysics*, vol. 39, no. 3, 347-383.
- Bour O., Davy, P., Darcel, C., Odling, N. E., 2002, A statistical scaling model for fracture network geometry, with validation on a multiscale mapping of a joint network (Hornelen Basin, Norway), *Journal of Geophysical Research*, vol. 107, no. B6, ETG 4-1 – 4-12.
- Chiles, J. P., 1988, Fractal and geostatistical methods for modeling of a fracture network, *Math. Geol.*, 20, 631–654.

- Doughty, C. and Karasaki, K., 2002, Flow and transport in hierarchically fractured rock, *Journal of Hydrology*, vol. 263, 1-2
- Gillespie, P.A., Howard, C.B., Walsh, J.J., Watterson, J., 1993, Measurement and characterization of spatial distributions of fractures, *Tectonophysics*, vol. 226, 113-141
- Hausdorff, F., 1919, Dimension und ausseres Mass, *Math. Ann.*, 79, 157
- La Pointe, L.R., 1988, A Method to Characterize Fracture Density and Connectivity Through Fractal Geometry, *Int. J. Rock Mech. Min. Sci. Geomech. Abstr.*, vol. 25, 421-429
- Mandelbrot, B.B., 1983, *The Fractal Geometry of Nature*, Freeman, New York, NY, 468pp.
- Marrett, R., Ortega, J. O., Kelsey C. M., 1999, Extent of Power-Law Scaling for Natural Fractures in Rock, *Geology*, vol. 27, no. 9, 799-802
- Odling, N. E., 1999, Variations in fracture systems geometry and their implications for fluid flow in fractured hydrocarbon reservoirs, *Petroleum Geoscience*, vol. 5, 373-384.
- Odling, N. E., 1997, Scaling and connectivity of joint systems in sandstones from western Norway, *Journal of Structural Geology*, vol. 19, no. 10, 1257-1271.
- Ouillon, G., Castaing, C., Sornette, D., 1996, Hierarchical geometry of Faulting, *Journal of Geophysical Research*, vol. 101, no. B3, 5477-5487.

- Sammis, G. C., Osborne, R.H., Anderson, J. L., Banerdt, M, White, P., 1986, Self-Similar Cataclasis in the Formation of Fault Gouge, *Pure Appl. Geophysics*, vol. 124, nos. 1/2, 53-78.
- Walsh, J.J., Watterson, J., 1993, Fractal Analysis of Fractal Patterns using the standard Box-counting Technique: valid and invalid methodologies, *Journal of Structural Geology*, vol. 15, no. 12, 1509-1512.
- Zhang, X., Sanderson, D. J., 1994, Fractal Structure and Deformation of Fractured Rock Masses, in Kruhl, J. H., ed., *Fractals and Dynamic Systems in Geoscience*, Springer-Verlag, Frankfurt, Germany, 421pp.
- Zhang, S., Zhou, X., 2000, A Review on the fractal of fault systems, *Journal of Guilin Institute of Technology*, vol. 20, no. 1, 84-88

APPENDIX I A

In our model the length distribution of the fractures at iteration i is given by:

$$N_{f_i} = 2(b-1)(b^2 - n)^i \dots\dots\dots(1)$$

$$l = 1/b^i \dots\dots\dots(2)$$

For a cumulative length count equation (2) can be written as:

$$cumN_{f_i} = \sum_{i=0}^i 2(b-1)(b^2 - n)^i = 2(b-1) \sum_{i=0}^i (b^2 - n)^i \dots\dots\dots(3)$$

summing as a geometric series we get:

$$cumN_{f_i} = 2(b-1) \frac{[1 - (b^2 - n)^{i+1}]}{[1 - (b^2 - n)]} \dots\dots\dots(4)$$

taking the log on both sides in equation (4) we get:

$$\log(cumN_{f_i}) = \log 2 + \log(b-1) + \log[1 - (b^2 - n)^{i+1}] - \log[1 - (b^2 - n)] \dots\dots\dots(5)$$

Now, slope of the line on the log (cumulative length) vs. log (number) plot is given by:

$$slope = \frac{\Delta \log cumN_f}{\Delta \log l} = \frac{\log cumN_{f_i} - \log cumN_{f_{i-1}}}{\log l_i - \log l_{i-1}} \dots\dots\dots(6)$$

from equations (2) and (5):

$$\log cumN_{f_i} - \log cumN_{f_{i-1}} = \log[1 - (b^2 - n)^{i+1}] - \log[1 - (b^2 - n)^i] \dots\dots\dots(7)$$

$$\log l_i - \log l_{i-1} = -i \log b - \{(i-1) \log b\} = -\log b \dots\dots\dots(8)$$

substituting equations (7) and (8) in equation (6):

$$slope = - \frac{\log \left[\frac{1 - (b^2 - n)^{i+1}}{1 - (b^2 - n)^i} \right]}{\log b} \dots\dots\dots(9)$$

therefore, for $i \rightarrow \infty$, the slope in the limit is:

$$\underset{i \rightarrow \infty}{Lt \text{ slope}} = - \underset{i \rightarrow \infty}{Lt} \frac{\log \left[\frac{1 - (b^2 - n)^{i+1}}{1 - (b^2 - n)^i} \right]}{\log b} = - \frac{\underset{i \rightarrow \infty}{Lt} \log \left[\frac{1 - (b^2 - n)^{i+1}}{1 - (b^2 - n)^i} \right]}{\underset{i \rightarrow \infty}{Lt} \log b} \dots\dots\dots(10)$$

invoking the relationship $\underset{x \rightarrow a}{Lt} f(g(x)) = f(\underset{x \rightarrow a}{Lt} g(x))$ equation (10) may be rewritten as:

$$\underset{i \rightarrow \infty}{Lt \text{ slope}} = - \frac{\log \underset{i \rightarrow \infty}{Lt} \left[\frac{1 - (b^2 - n)^{i+1}}{1 - (b^2 - n)^i} \right]}{\log b} \dots\dots\dots(11)$$

dividing the numerator and denominator terms by $(b^2 - n)^i$ we get:

$$\underset{i \rightarrow \infty}{Lt \text{ slope}} = - \frac{\log \underset{i \rightarrow \infty}{Lt} \left[\frac{\{1/(b^2 - n)^i\} - (b^2 - n)}{\{1/(b^2 - n)^i\} - 1} \right]}{\log b} \dots\dots\dots(12)$$

$$\therefore \underset{i \rightarrow \infty}{Lt \text{ slope}} = - \frac{\log(b^2 - n)}{\log b} \dots\dots\dots(13)$$

The RHS term in equation (13) is same as the expression for the theoretical fractal dimension, D of our model given by equation (1) in chapter 2.

APPENDIX I B -TABLES

Table 1.1 Percentage errors in evaluating D_b for synthetic patterns using whole range of data points and points turned off for $r < proxy\ r_{min}$ and $r < r_{min}$

i	D	D_b wholerange	% error: whole range	$D_b\ r_{min}$	% error: r_{min}	$D_b\ proxy\ r_{min}$	% error: $proxy\ r_{min}$
1	1.58	1.07	-32.49	1.43	-9.78	1.53	-3.47
2	1.58	1.13	-28.70	1.57	-0.94	1.52	-4.10
3	1.58	1.22	-23.03	1.62	2.21	1.61	1.58
4	1.58	1.31	-17.35	1.61	1.58	1.62	2.21
5	1.58	1.40	-11.67	1.62	2.21	1.62	2.21
6	1.58	1.48	-6.62	1.62	2.21	1.62	2.21

Table 1.2 Odling's (1997) maps: scales, $proxy\ r_{min}$ (in pixels), $proxy\ r_{min}$ (in meters), modified box-counting dimension D_b and capacity dimension, D^* (Bour et al., 2002)

no	map name	area	scale	$proxy\ r_{min}$ (m)	D_b	D^*
1	horn_ya	18m x 18m	1:102	0.35	1.80 ± 0.05	1.80 ± 0.1
2	horn_yb	55m x 55m	1:313	0.81	1.82 ± 0.04	1.77 ± 0.08
3	horn_yc	90m x 90m	1:511	1.33	1.82 ± 0.05	1.80 ± 0.05
4	horn_sa	90m x 90m	1:511	1.33	1.81 ± 0.05	1.80 ± 0.1
5	horn_sb	180m x 180m	1:1023	2.4	1.82 ± 0.04	1.82 ± 0.1
6	horn_sc	360m x 360m	1:2045	3.62	1.84 ± 0.04	1.85 ± 0.1
7	horn_sd	720m x 720m	1:4091	7.25	1.84 ± 0.04	1.88 ± 0.1

Table 1.3 Barton's maps: reported l_{min} , $proxy\ r_{min}$ (in meters) for uncropped maps, $proxy\ r_{min}$ for cropped maps, D_b evaluated by Barton (1995), D_b evaluated using whole range of data points, D_b (fractal dimension from uncropped maps) and $(D_b)_c$ (fractal dimension from cropped maps)

maps	l_{min} (m)	$proxy\ r_{min}$ (m)	$proxy\ r_{min}\ c$ (m)	D_b barton	D whole	D_b	$(D_b)_c$
a	0.25	0.32	0.31	1.52	1.55	1.64 ± 0.01	1.62 ± 0.03
b	0.5	0.74	0.97	1.38	1.45	1.56 ± 0.02	1.58 ± 0.04
c	0.39	0.36	0.36	1.5	1.54	1.62 ± 0.02	1.66 ± 0.03
d	0.59	1.43	1.6	1.61	1.61	1.71 ± 0.01	1.75 ± 0.05
e	0.23	0.4	0.43	1.59	1.56	1.74 ± 0.02	1.76 ± 0.05
f	0.24	0.47	0.65	1.54	1.54	1.64 ± 0.03	1.65 ± 0.03
g	0.2	0.17	0.17	1.7	1.65	1.77 ± 0.02	1.78 ± 0.02
h	1.7	1.56	2.61	1.5	1.55	1.62 ± 0.02	1.77 ± 0.08
i	0.09	0.2	-	1.6	1.63	1.75 ± 0.04	-
j	0.12	2.35	2.63	1.5	1.67	1.79 ± 0.02	1.79 ± 0.04
k	0.2	0.36	0.44	1.58	1.68	1.78 ± 0.02	1.83 ± 0.04
l	0.08	0.15	0.31	1.52	1.58	1.66 ± 0.02	1.78 ± 0.11
m	53	306.92	-	1.49	1.49	1.75 ± 0.06	-
n	0.4	1.28	1.5	1.48	1.5	1.69 ± 0.02	1.73 ± 0.05
o	26	46.16	54.98	1.52	1.61	1.7 ± 0.02	1.75 ± 0.03
p	99000	103000	-	1.32	1.47	1.63 ± 0.02	-
q	0.0005	0.000412	0.000438	1.58	1.47	1.69 ± 0.03	1.72 ± 0.03

APPENDIX I C - FIGURES

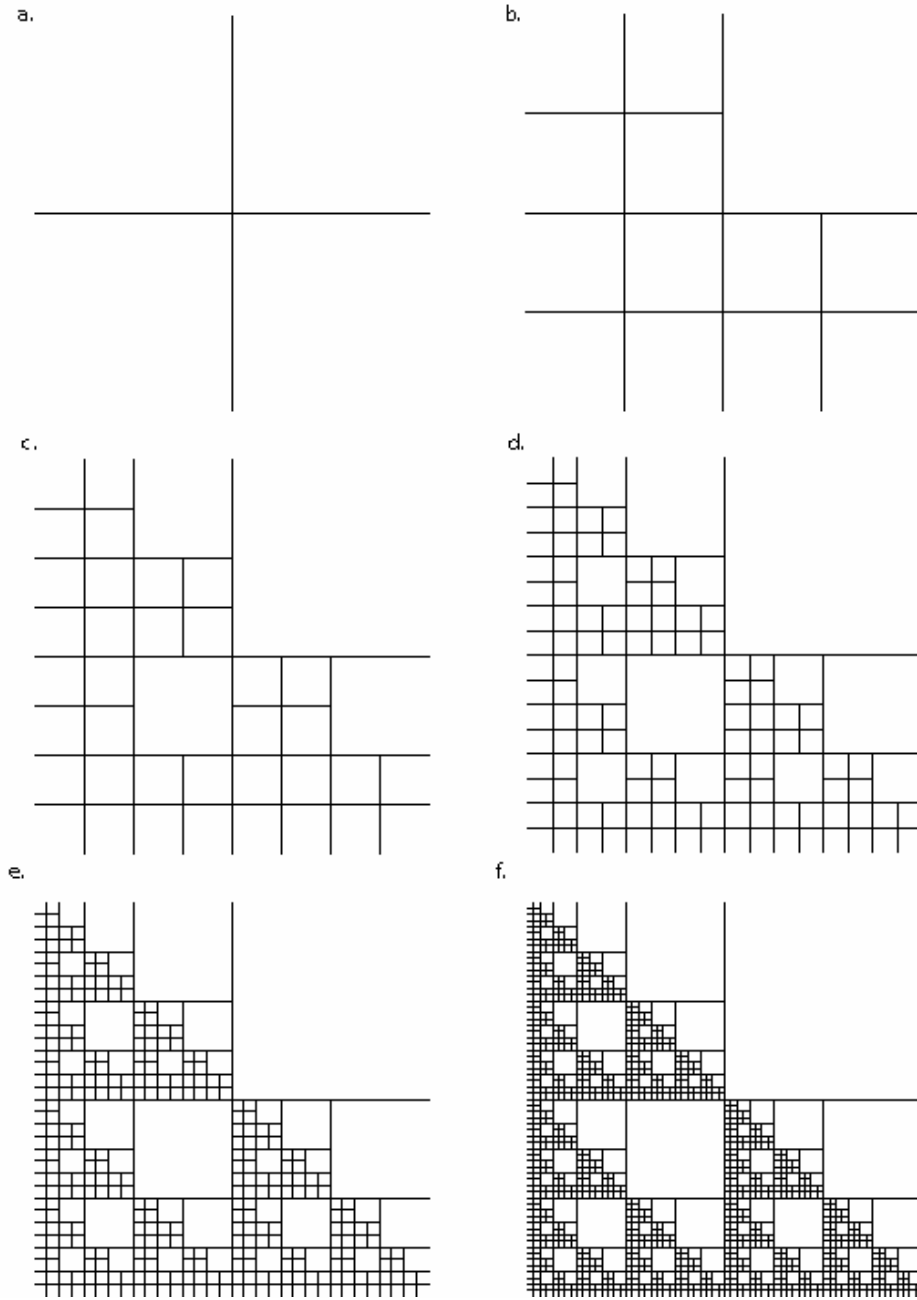


Figure 1.1 Construction of a deterministic Sierpinski lattice with $b=2$ and $n=1$: (a) basic template $i = 0$ with two fractures of length 1, (b) $i = 1$: addition of fractures of length $1/2$, (c) $i = 2$: addition of fractures of length $1/4$, (d) $i = 3$: addition of fractures of length $1/8$, (e) $i = 4$: addition of fractures of length $1/16$ (f) $i = 5$: addition of fractures of length $1/32$

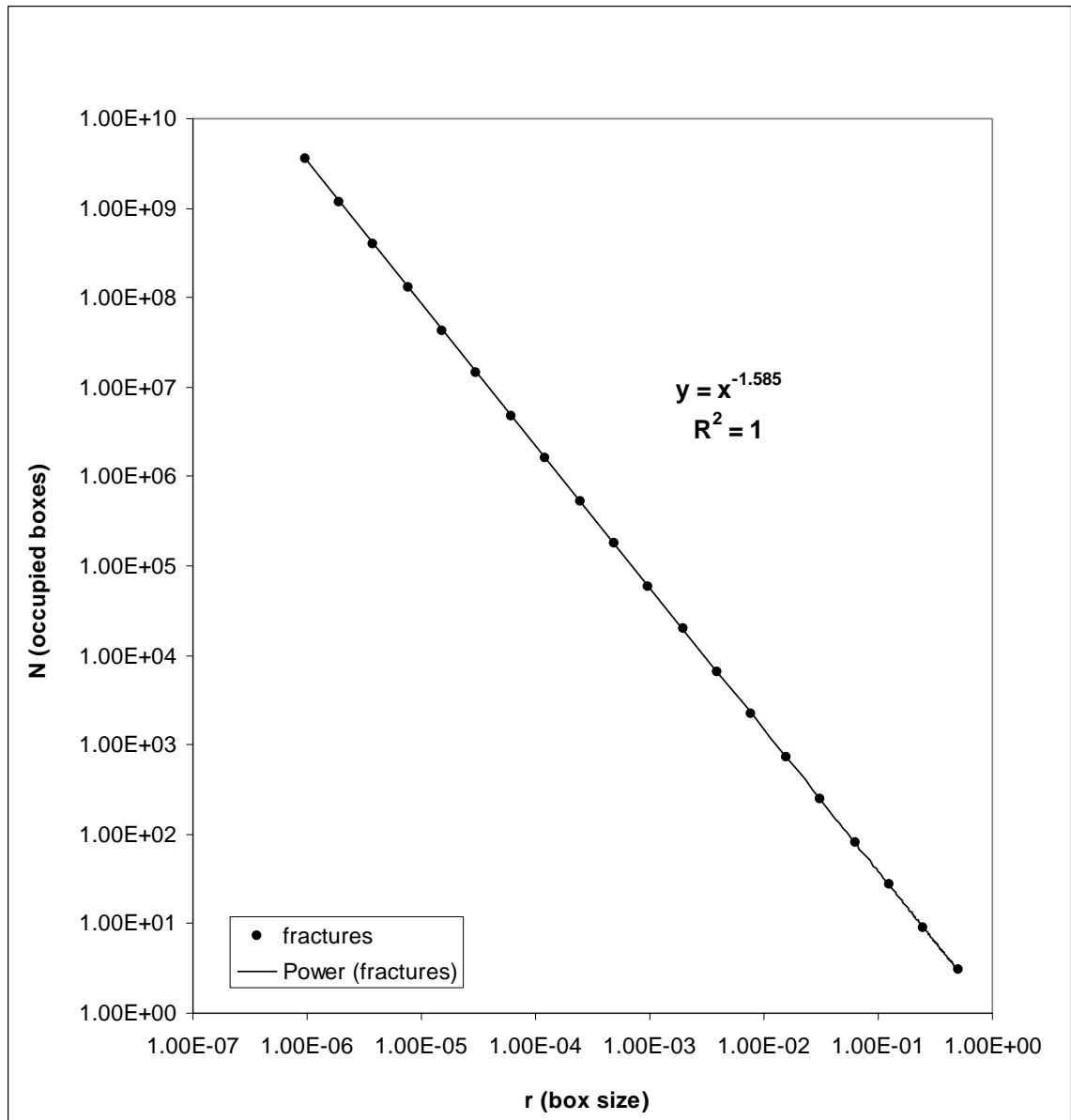


Figure 1.2 Analytical box-counting showing N (no. of boxes) vs. r (box-size) plots for fractures in synthetic pattern with $b=2$, $n=1$ and $i=20$

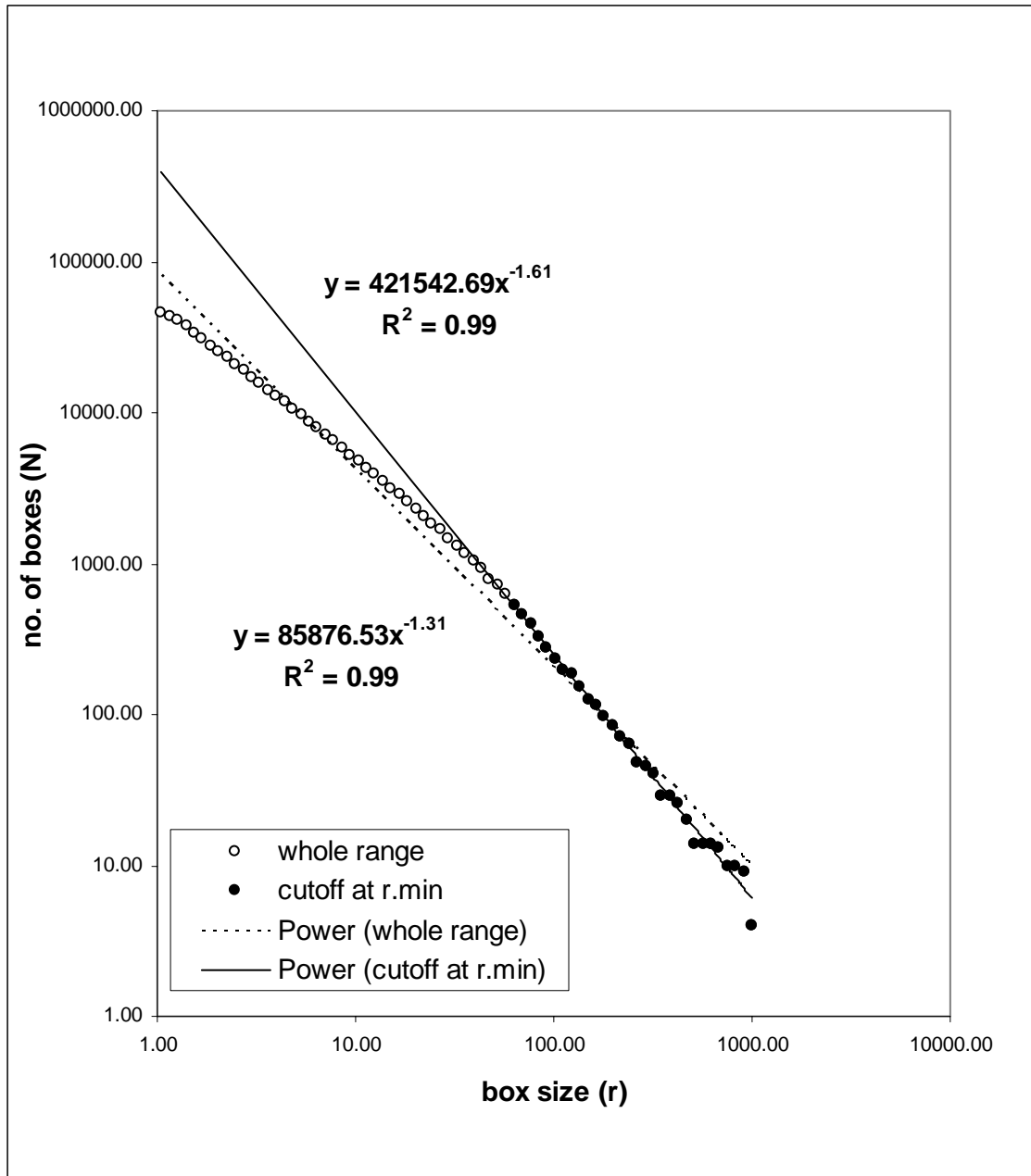


Figure 1.3 Plot showing N (no of boxes) vs. r (box size) for synthetic pattern with $b=2$, $n=1$, $i=4$ with whole range of data points and those for which $r < r_{min}$, “turned off”

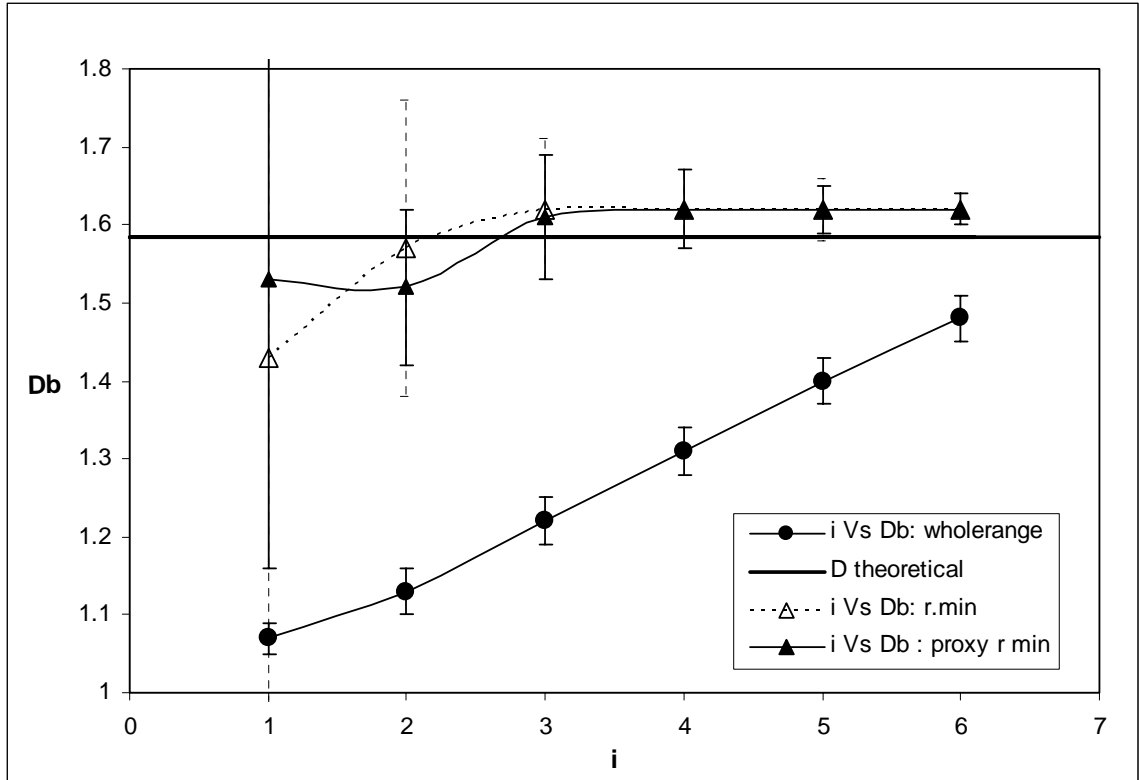


Figure 1.4 Plot showing variation of D_b with i for synthetic patterns $b=2$, $n=1$: D_b ($\pm 95\%$ confidence intervals) computed using whole range of box-sizes, box-sizes larger than the r_{min} and box-sizes larger than the *proxy* r_{min}

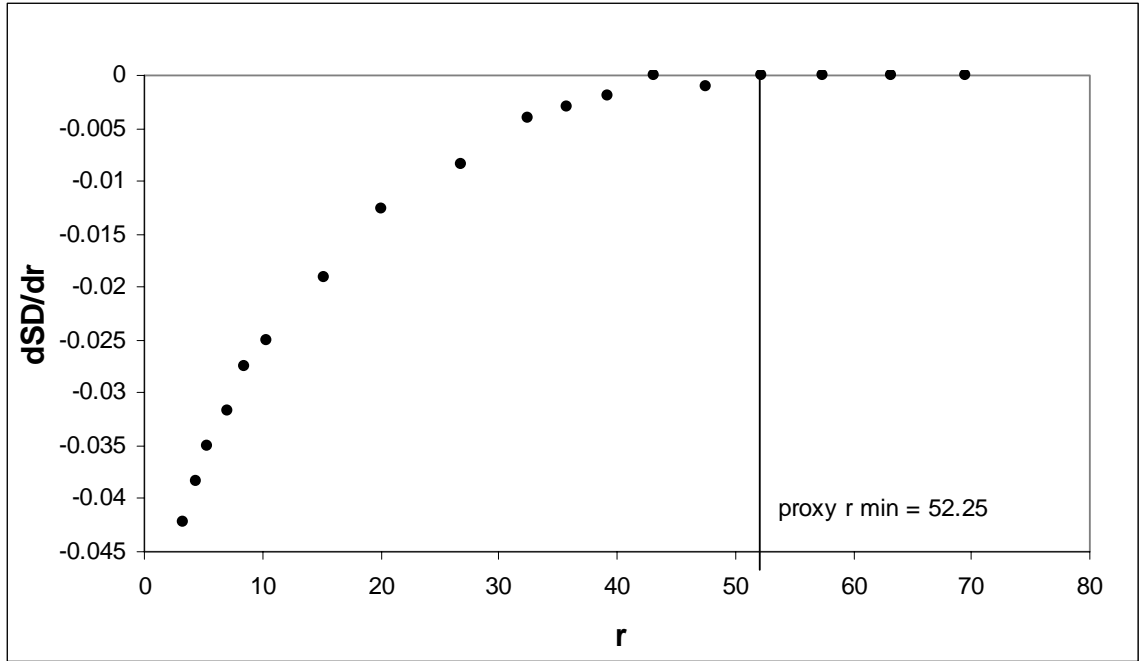


Figure 1.5 Plot showing $d(SD)/dr$ vs. r for synthetic pattern $b = 2$, $n = 1$, $i = 4$ used for finding the *proxy* r_{min} . (theoretical $r_{min} = 63.23$)

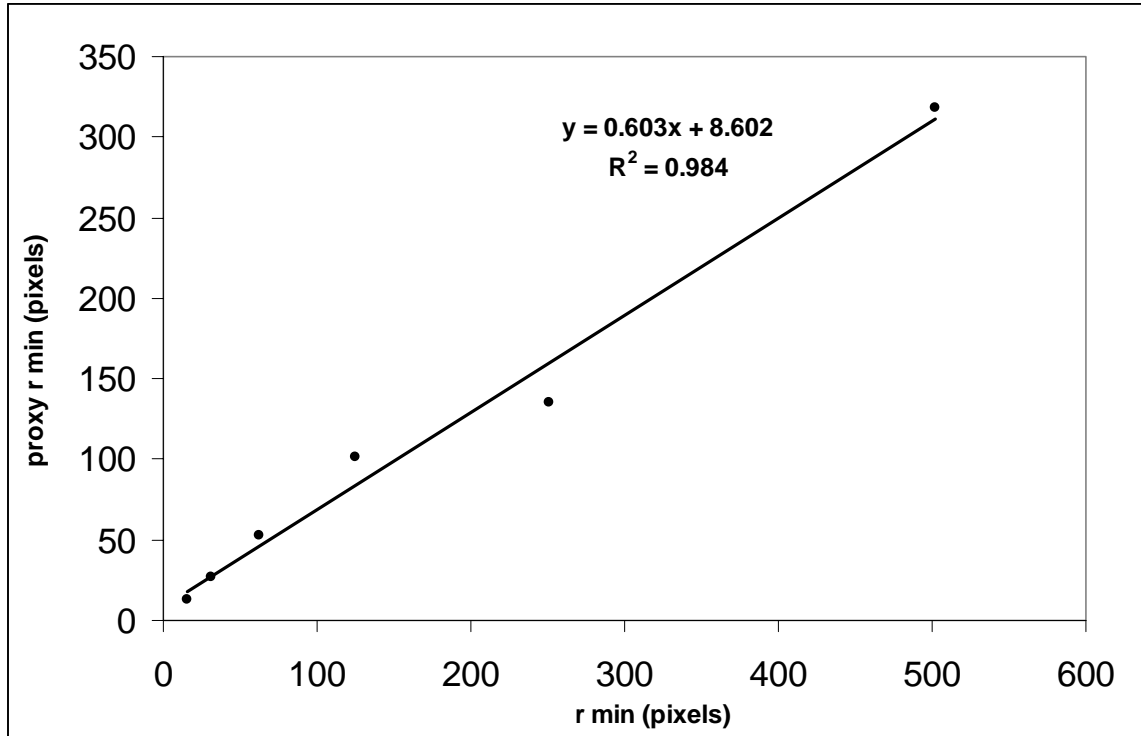


Figure 1.6 Plot showing relationship between r_{min} and $proxy\ r_{min}$ for synthetic pattern with $b = 2$, $n = 1$ at different iteration levels ($i = 1 - 6$)

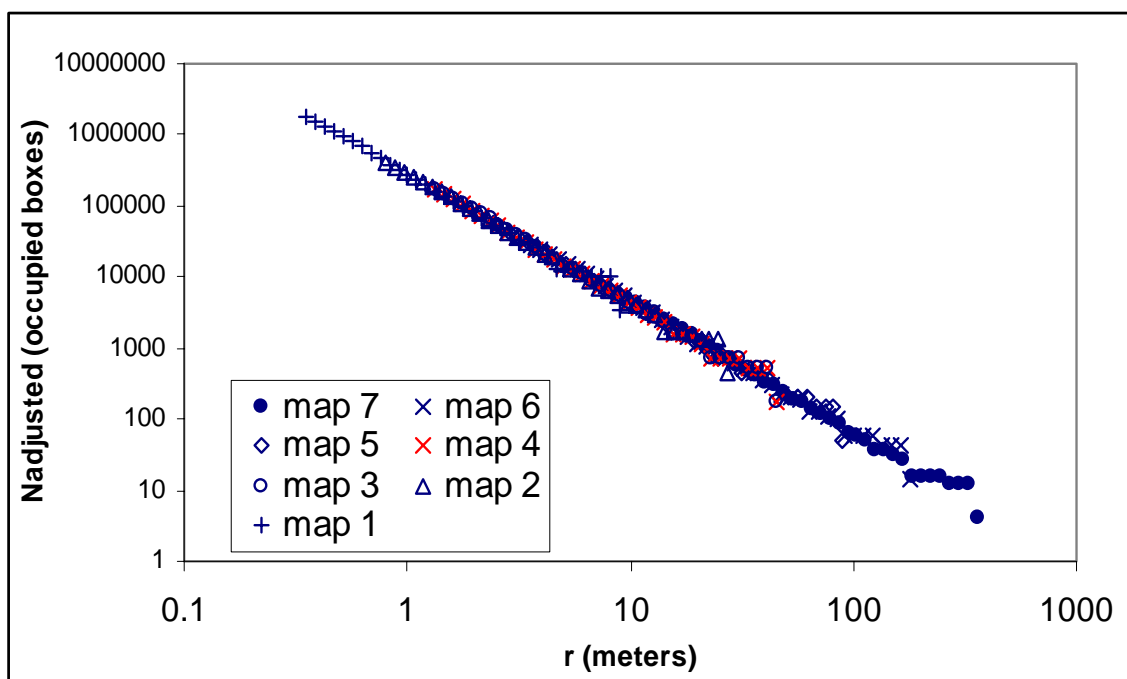


Figure 1.7 $N_{adjusted}$ vs. r_m for maps 1-7 from Odling (1997)

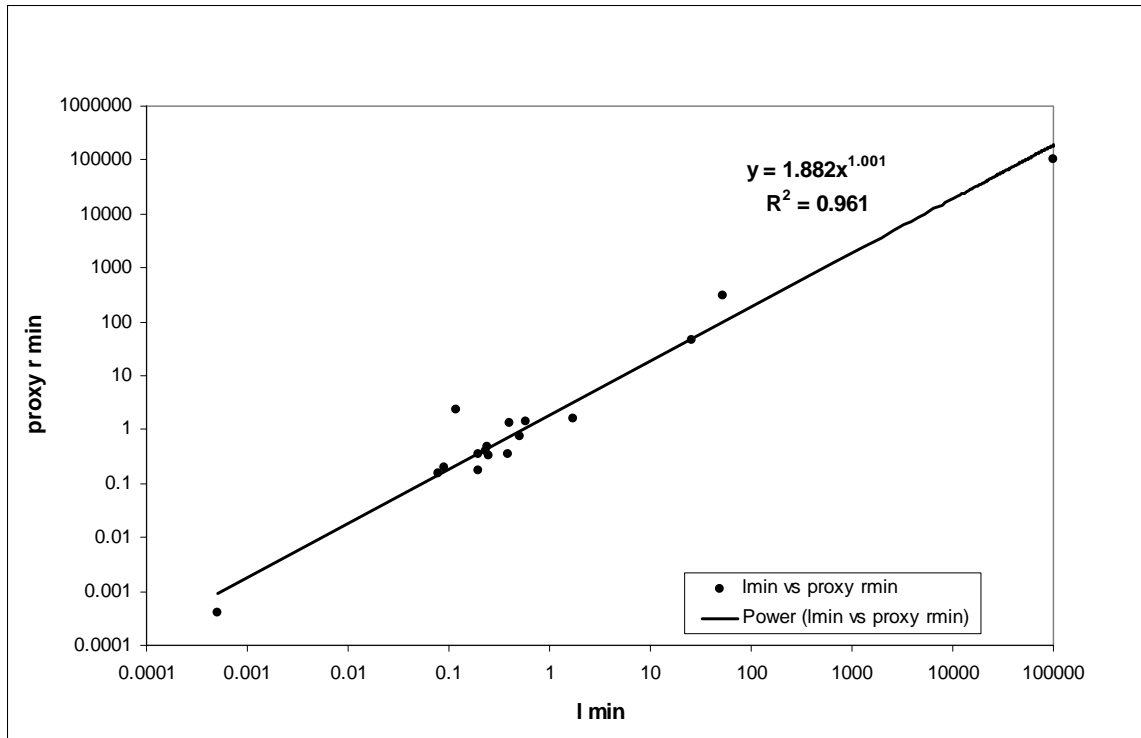


Figure 1.8 Plot showing relationship between l_{min} and $proxy\ r_{min}$ for Barton's (1995) maps

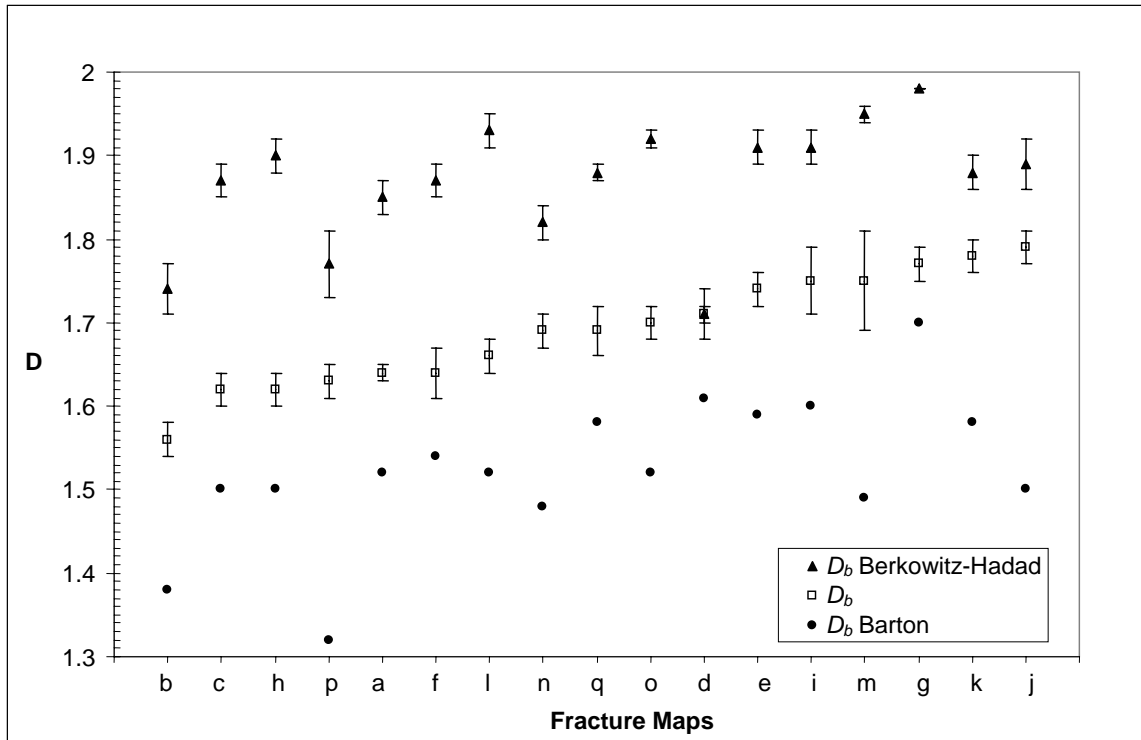


Figure 1.9 Comparison of fractal dimensions of Barton's (1995) maps as computed by Barton (1995), Berkowitz and Hadad (1997) and using the improved method

PART II

Lacunarity Analysis of Fracture Networks

1. INTRODUCTION

The importance of fractures and their pattern geometries cannot be overemphasized since they play a significant role in geological systems ranging from crustal fluid flow to studies of earthquakes. Geostatistical techniques, semi-variograms in particular, have been widely employed for fracture characterization (e.g., La Pointe and Hudson, 1985; Chiles, 1988 and Marrett et al., 2006). Over the past two decades some investigations have quantified the size scaling and spatial properties of fracture networks with fractal descriptors. For example, Barton and Larsen (1985) defined the geometry of fracture patterns with a fractal dimension using the “box-counting” method. A persistent problem in such characterizations however, is that fracture patterns having different appearances can have the same fractal dimension. The conclusion of part I therefore posed the question as to whether any other parameter can be used to uniquely quantify a particular pattern. We address this basic question in part II by considering our synthetic fractal-fracture patterns and the data set from the Hornelen basin, Norway (Odling, 1997). In this part we step aside from the idea of a fractal dimension and instead consider fracture patterns from a more generalized point of view.

Early studies about fractal properties gave way to the new concept of lacunarity. Mandelbrot (1983) defined this characteristic as the degree of clustering in a pattern. For instance, in a fracture pattern, if a large unfractured area is present, the pattern will have a high lacunarity value. Allan and Cloitre (1991) proposed a method for quantifying the lacunarity of any pattern using the gliding-box method. Following this work, Plotnick et al. (1996) analyzed a suite of geological (γ -ray peaks from well logs) and ecological data and showed that lacunarity may be used as a general tool for spatial analysis of fractal, multifractal and non-fractal data sets well as. Turcotte (1997) extended the idea of the gliding box method to 2 dimensions and calculated the lacunarity of a second-order Sierpinski carpet. Chen (1997) used this concept for studying zinc concentration values. Along with the gliding box algorithm, another technique, the sandbox algorithm (Chappard et al., 2001) has been employed for determining lacunarities of soil microstructures (Pendleton et al., 2005). However, neither the gliding box nor the sandbox method has been previously used for determining the lacunarities of fracture networks.

The purpose of the present work is to use the gliding box technique to compute the lacunarities of fracture networks that have similar fractal dimensions and to investigate the scale range over which fracture networks might be self-similar. A MATLAB code was written for analyzing fracture patterns using the gliding-box algorithm (Appendix II C). Two deterministic fractal-fracture models, and a set of eleven random ones, all generated using two MATLAB codes (Appendices II A and B) were analyzed. In addition, a set of 7 fracture maps from the Hornelen basin, Norway (Odling, 1997) was evaluated to determine the ability of this method to discriminate between patterns with similar fractal dimensions.

2. SYNTHETIC FRACTAL-FRACTURE PATTERNS

A suite of deterministic and random fractal-fracture patterns was constructed using hierarchical fracture networks made up of line segments in 2D. The networks were generated using MATLAB (Appendices II A and B) and are essentially generalized versions of Sammis' (1986) model. Three basic parameters are used to for generating the patterns – scaling factor: b , number of blocks not iterated at each step: n , and iteration: i .

For the first network, a value of $b = 2$ is used such that the initial square template consists of two orthogonal fractures dividing the whole area into four blocks each with a side of length 0.5 (Fig 2.1a; all tables and figures in appendices II E-F). We call this the initiator such that $i = 0$. At each level $n = 1$ block is left unfractured and the others are reiterated by shrinking this template ($i = 0$) by a factor of 2, replicating it $b^2 - n = 2^2 - 1 = 3$ times and finally superimposing the resulting patterns on the original template as shown in Fig 2.1b. This process is then repeated for each of the 0.5 length templates (Fig 2.1c), then for each of the resulting 0.25 and 0.125 length templates and so on until a sequence of 5 patterns is produced at for $i=0$ to 4 as seen in Fig 2.1a-e. Hereafter, the pattern will be referred to as **b2n1i4_det**. This pattern was “randomized” by using a probability function for choosing the “un-fractured” block from the four initial blocks and repeating the process until $i=4$ (Fig 2.1f) and this pattern is named **b2n1i4_ran**. Ten such random patterns were generated. A second deterministic fractal-fracture pattern (Fig 2.2a) and its random counterpart (Fig 2.2b) were generated likewise for $b = 4$, $n = 7$ and $i = 2$. These patterns are named as **b4n7i2_det** and **b4n7i2_ran**, respectively. The iteration in this case is done only until $i=2$ such that the smallest fracture length, l_{min} is the same size in both models i.e.:

$$l_{min} = \frac{1}{b^i} \dots\dots\dots (1)$$

$$b = 2, i = 4, l_{min} = \frac{1}{2^4} = \frac{1}{16}$$

$$b = 4, i = 2, l_{min} = \frac{1}{4^2} = \frac{1}{16}$$

The theoretical fractal dimension, D of the synthetic patterns is:

$$D = \frac{\log(b^2 - n)}{\log b} \dots\dots\dots(2)$$

$$b = 2, n = 1$$

$$D = \frac{\log(2^2 - 1)}{\log 2} = \frac{\log 3}{\log 2} = 1.585$$

$$b = 4, n = 7$$

$$D = \frac{\log(4^2 - 7)}{\log 4} = \frac{\log 9}{\log 4} = \frac{\log 3^2}{\log 2^2} = \frac{\log 3}{\log 2} = 1.585$$

Although the two patterns have the same fractal dimension, they do not look identical (Figs 2.1, 2.2). For that matter, it may be easily proved that for any set of b and n such that:

$$b = 2^m \dots\dots\dots(3a)$$

$$n = 4^m - 3^m \dots\dots\dots(3b)$$

where m is any positive integer, the fractal dimension of the pattern will be $D = 1.585$. For the two particular models constructed here, $m=1$ and 2 respectively. Consequently, many possible synthetic patterns would have the same fractal dimension, but may be quite different in appearance. Our purpose is to characterize this difference.

3. THEORY

In this section we introduce the concept of translational invariance and use it to explain lacunarity. We then describe the gliding box algorithm to show how lacunarity may be quantified and that in essence it is a ratio of the variance to the mean of a pattern.

3.1 Translational Invariance

A simple 32×32 square grid (Fig 2.3) will map onto itself if a copy of it is made and moved by one unit so that the original cannot be distinguished from the translated copy. This is called translational invariance. Quite obviously, this property is not observed in a slightly more complicated pattern like `b2n1i4_ran` because unlike the simple grid, this pattern has heterogeneity. The deviation of a pattern from translational invariance can thus be conceived as a measure of the degree of heterogeneity of texture. This property is highly scale dependent because sets that are homogeneous at a larger scale can be heterogeneous at smaller scales and vice-versa.

3.2 Lacunarity

In simple terms, lacunarity (L) is the degree of clustering in a pattern. It is actually a measure of the degree to which a set is *not* translationally invariant (Allan and Cloitre, 1991). This means to say that for translationally invariant sets, $L = 1$ and for non-translationally invariant sets $L > 1$. As every pattern may have some sort of heterogeneity, lacunarity can be a property of both fractal and non-fractal patterns.

3.3 The Gliding-box Algorithm

This algorithm puts the investigated pattern on an underlying lattice and then moves a window of a given length, r translated in unit increments of the chosen lattice (Allan and Cloitre, 1991). Consider the four linear patterns in Fig 2.4. Each is of total length $r_t = 27$ and has 8 occupied units distributed in different ways: (a) almost uniform; (b) deterministic fractal – cantor dust; (c) random fractal – cantor dust; and (d) clustered. The

underlying lattice has a mesh size of unit length and is the same as the one on which the sets are built. As the window glides across, the total number steps covered is given by:

$$N(r) = (r_t - r + 1)^E \dots\dots\dots(4)$$

E is the Euclidean dimension of the pattern. Here $E = 1$; for a window size of $r = 9$, we have:

$$N(9) = (27 - 9 + 1) = 19.$$

The frequency of the distribution of the masses (occupied units) in the window of size r containing s occupied units is given by $n(s, r)$ (Fig 2.5). This can be converted to a probability distribution as:

$$Q(s, r) = n(s, r)/N(r) \dots\dots\dots(5)$$

The 1st and 2nd moments, which are related to the mean and variance of the distribution of this probability function, are:

$$M_1(r) = \sum s.Q(s, r) \dots\dots\dots(6a)$$

$$M_2(r) = \sum s^2.Q(s, r) \dots\dots\dots(6b)$$

The lacunarity, L is (Allan and Cloitre, 1991):

$$L(r) = M_2(r)/[M_1(r)]^2 \dots\dots\dots(7)$$

Lacunarity is thus the dimensionless representation of the variance to mean ratio at a given scale (Plotnick et al., 1996).

The $L(r)$ of a pattern has upper and lower bounding values. Consider ϕ as the fraction of sites occupied (this is the *same* as the fracture porosity values for our fracture patterns). In Fig 2.4 for example, $\phi = 8/27$. It may be easily proved that $Q(1, 1) = \phi$, in all cases (Plotnick et. al. 1996). The lacunarity $L(1) = M_2(1)/[M_1(1)]^2 = \phi/\phi^2 = 1/\phi$. From Fig. 2.4, $L(1) = 27/8 = 3.33$ (Fig 2.6). For $r = r_t$, $M_1(r_t) = 1$, and $M_2(r_t) = 1$, therefore from

equation (7), $L(r_i) = I$. To summarize, the upper bound $L_{upper} = I/\phi$ and the lower bound is $L_{lower} = I$

The L -values can be plotted versus the window sizes, r , to yield the lacunarity curve of a pattern (e.g. Fig 2.6). It can be further shown that on a log-log scale patterns that are self-similar monofractals plot on straight lines, from the slope of which their fractal dimensions may be found (Allan and Cloitre, 1991). This also means that the lacunarity curves can be used to investigate the range of scales for which a pattern may be fractal because the curve should be a straight line over this range.

4. DATA ANALYSIS AND RESULTS

The gliding-box technique has been applied to our synthetic patterns and a set of natural fracture maps published by Odling (1997). For natural data sets, Allan and Cloitre (1991) recommended that the underlying lattice should be the array of pixels that define the image. To be consistent, we chose the pixels to be the underlying lattice for both the synthetic and the natural patterns. A square window edge length r glides across the pattern (Fig 2.7) recording the number of steps $n(s,r)$ with s occupied pixels that are inside and on the box boundaries and the lacunarity $L(r)$ is calculated (equation 7). A MATLAB code written by Jung-woo Kim was modified for this purpose (Appendix II C). The program computes the $L(r)$ value for a given r from bitmap image files. Before we used it for our purpose, it was tested on a second order Sierpinski carpet (Mandelbrot, 1983) that had been previously evaluated for its L value (Turcotte, 1997), using equations (4) to (7). It returned a similar value (within 0.4%) to that given by the analytical method employed by Turcotte (1997) thus demonstrating its effectiveness in computing the lacunarity parameter. Following this test, the $L(r)$ values for our fracture patterns were found and were plotted against the r -values thus yielding the lacunarity curve. Fracture porosity is another parameter that was evaluated using a MATLAB code (Appendix II D). This is a ratio between the number of the occupied pixels that constitute the fractures and the total number pixels in the pattern. This parameter may be used in conjunction with the fractal dimension, *proxy* r_{min} and lacunarity values for comparing patterns.

4.1 Synthetic Fracture Networks

The lacunarity curves (Fig 2.8) for each of the five patterns: b2n1i4_det, b2n1i4_ran, b4n7i2_det, b4n7i2_ran and trans-inv (translationally invariant simple 32 X 32 grid) show that b4n7i3_det always has the greatest lacunarity, possibly because of the clustering of un-fractured blocks in the upper right corner (see Fig 2.2a). They occupy about 7/16 of the entire area as opposed to 1/4 i.e. 4/16 for b2n1i4_det. Interestingly, the randomized version, b4n7i2_ran shows the lowest lacunarity profile because the blocks, each individually occupying 1/16 of the entire area, are randomly dispersed within the pattern. Also, as expected, the lacunarity curve for the trans-inv pattern plots along the line $L(r) =$

1. This result further bolsters the soundness of our code for calculating the lacunarities and corroborates the fact that lacunarity plots can successfully demonstrate differences in heterogeneities amongst patterns.

In another approach, 10 random realizations of b2n1i4 were generated and their lacunarities measured. The mean lacunarities are plotted versus the r along with the standard deviations of $L(r)$ for each r (Fig 2.9). Given that $L(r)$ has a lower bound of 1 and an upper bound of $1/\phi$ (ϕ being the porosity fraction and is *same* for *all* the random patterns) it is not really surprising that the standard deviation bars become smaller at the ends where L reaches it's limiting values which are *same* for all of the realizations.

The results for the synthetic patterns show that the fracture-porosities differ for patterns with distinct sets of b and n , although there was no change in this parameter for the deterministic and random counterparts of a particular b, n pair (Table 2.1). Additionally, it cannot be overemphasized that *all* of these patterns possess the *same* fractal dimension ($D=1.585$).

4.2 Natural Fracture Networks

Lacunarity curves were computed for a suite of 7 nested fracture patterns mapped in the Hornelen basin, Norway (Odling, 1997). Each pattern is a subset of a larger pattern (Fig 1, Bour et al., 2002) and is mapped from a lower elevation, such that it represents a limited range of joint trace lengths that is controlled by the resolution of the image. The original 7 maps were received as encapsulated postscript files from Dr Odling. They were then converted into bitmap images of 150dpi resolution using Adobe Illustrator (Appendix A). We previously evaluated these maps for their fractal character and found that they do display self-similarity. Details about the scales, minimum fracture sizes and fractal dimensions of the mapped areas are in documented in table 2.2.

These patterns were particularly chosen keeping in mind our objective of differentiating between fracture patterns that look different but have similar fractal dimensions. Obviously, if one is essentially a scaled down version of the other and the pattern is self-similar all the 7 maps should have the same fractal dimension (table 2.2). The lacunarity curves (Fig 2.10) for these maps were evaluated only up to $r = 100$ because for larger box-sizes their differences tend to become smaller and for all the maps the $L(r)$ tends to unity. It can be seen that the curves differ from each other because although they have similar shapes, they “spread out” on the $L(r)$ vs. r plot. The general trend is, the greater the resolution (smaller the scale of the map), the higher the lacunarity. This result means that the natural pattern is more clustered in the smaller scale maps. Visual inspection of the patterns (Appendix A) supports this interpretation because the smaller scale maps have larger unfractured areas as opposed to the large scale ones where the fractures tend to be more randomly distributed (personal communication Noelle Odling, March 06 2006).

The fracture porosity tends to decrease with decreasing scale because with greater lacunarity, the patterns are more clustered in the smaller scale maps and as a result, more intersections exist that decreases the porosity. The theoretical L_{upper} value ($L_{upper} = 1/\phi$) has a high correlation with the empirical $L(10)$ for all the maps 1-7 (Fig 2.11) which further underscores the idea that the fracture porosity decreases with clustering (lower lacunarity).

5. DISCUSSION AND CONCLUSIONS

This work presents a number of new and important ideas and concepts. It has already been shown in earlier research that the degree of heterogeneity in a pattern can be quantified by using lacunarity as a parameter. The present study shows that this concept may be applied in the area of fracture research for distinguishing between different fracture networks that may have similar fracture-porosity and fractal dimension values and for studying their scaling characteristics.

Lacunarity is the extent to which a set is *not* translationally invariant. Sets that are completely translationally invariant will have a lacunarity of unity irrespective of the size of the gliding window. The lacunarity parameter, $L(r)$ is a dimensionless representation of the variance to mean ratio and can be applied in a general manner to fractals and non-fractals alike and helps in distinguishing between the two. Since translational invariance is a highly scale dependent property, lacunarity can delineate the presence of heterogeneities at any scale. In fact, not only does it identify the presence of self-similarity in a set, but being scale dependent it reveals the *range* of self-similarity as well.

Different synthetic fractal-fracture patterns with a single known theoretical fractal dimension, but with variability in their spatial organization, can be distinguished from each other by their lacunarity curves. More randomly distributed fractal-fracture networks tend to display lower lacunarities and hence are less clustered than their deterministic counterparts.

Our study of a suite of 7 nested natural fracture patterns (Odling, 1997) shows that the same fracture network at different scales can display variability in its clustering attributes. Although the 720m x 720m map is a self-similar one and had the same fractal dimension at different scales, there is a systematic variability in the lacunarity curves. In general, the larger the scale, the lower the resolution, and lower is lacunarity suggesting that the fractures appear to be more clustered at smaller scales and more randomized at larger scales. In addition, lower lacunarity values were associated with higher fracture porosities (Table 2.2).

The results presented in this work can potentially open up a myriad vistas for future research. Firstly, it would be an interesting exercise to look into the deviation of the fractal dimensions, arrived at by the gliding-box method, from the true theoretical values. In this context, one might want to revisit the derivation of equation 12 presented by Allan and Cloitre (1991). Additionally, more research is needed in order to address questions on the choice of the underlying lattice over which a set is laid before subjecting it to the gliding-box algorithm. It could be either the array of pixels that define a digitized pattern or simply the lattice on which a set is built. The former however, seems to be a better choice for characterizing the clustering of fracture patterns without any preconceived notion about their self-similarity.

References

- Allain, C. and Cloitre, M., 1991, Characterizing the lacunarity of random and deterministic fractal sets, *Phys. Rev. A*, vol. 44, no. 6, 3552-3558
- Barton, C. C., 1985, Fractal Geometry of two-dimensional fracture networks at Yucca Mountain, Southwestern Nevada, *Proceedings of the International Symposium on fundamentals of Rock Joints*, 77-84
- Bour O., Davy, P., Darcel, C., Odling, N. E., 2002, A statistical scaling model for fracture network geometry, with validation on a multiscale mapping of a joint network (Hornelen Basin, Norway), *Journal of Geophysical Research*, vol. 107, no. B6, ETG 4-1 – 4-12.
- Chappard, D., 2001, Fractal dimension of trabecular bone: comparison of three histomorphometric computed techniques for measuring the architectural two-dimensional complexity, *J. Pathology*, 195(4), 515-521.
- Chen, Q., 1997, Multifractal Modeling and Lacunarity Analysis, *Math. Geol.*, vol. 29, no. 7, 919-932.
- Chiles, J. P., 1988, Fractal and geostatistical methods for modeling of a fracture network, *Math. Geol.*, vol. 20, no. 6, 631–654.
- La Pointe, P.R. and Hudson, J.A., 1985, Characterization and Interpretation of Rock Mass Joint Patterns, *Geological Society of America*, Special Paper 199.
- Mandelbrot, B.B., 1983, *The Fractal Geometry of Nature*, Freeman, New York, NY, 468pp

- Marrett, R., Gale J., Gomez, L.A., 2006, Spatial Arrangement of Fracture Arrays III: Correlation Analyses (in press), *Journal of Structural Geology*.
- Odling, N. E., 1997, Scaling and connectivity of joint systems in sandstones from western Norway, *Journal of Structural Geology*, vol. 19, no. 10, 1257-1271.
- Pendelton, D.E., Dathe, A., Baveye, P., 2005, Influence of image resolution and evaluation algorithm on estimates of the lacunarity of porous media, *Phys. Rev. E*, vol. 72, no. 4, 041306-1-9
- Plotnick, R.E., Gardner, R.H., Hargrove, W.W., Prestegard, K., Perlmutter, M., 1996, Lacunarity Analysis: A General Technique for the Analysis of Spatial Patterns, *Phys. Rev. E*, vol. 53, no. 5, 5461-5468
- Sammis, G. C., Osborne, R.H., Anderson, J. L., Banerdt, M, White, P., 1986, Self-Similar Cataclasis in the Formation of Fault Gouge, *Pure Appl. Geophysics*, vol. 124, nos. 1/2, 53-78
- Turcotte, D. L., 1997, *Fractals and Chaos in Geology and Geophysics*, Cambridge U. Press, New York, 398pp.

APPENDIX II A

```
% Deterministic Fractal as Line
% dfln(maxit,rulmat)
% output : [Figure]
% maxit   = maximum iteration number
% rulmat  = rule as a square matrix

% by Kim, Jung-Woo (2005)
% modified by Ankur Roy (2005)

function [] = dfln(maxit,rulmat,lwidth)

[br bc] = size(rulmat);

if maxit ~= abs(fix(maxit)) | rulmat ~= abs(fix(rulmat)) | br ~= bc
    disp('!!!! Wrong Input... Try it again... !!!!!');
    return;
end
Figure;

matold = 0;
for it = 1:maxit
    [nrow ncol] = size(matold);
    matnew = ones(br^it,br^it);
    for i = 1:nrow
        for j = 1:ncol
            if matold(i,j) == 0
                for bb = 1:br-1
                    hh = line([(j-1)/br^(it-1)      j/br^(it-1)],...
                             [(i-1)/br^(it-1)+bb/br^it  (i-1)/br^(it-1)+bb/br^it]);
                    set(hh, 'LineWidth',lwidth, 'Color',[0 0 0])
                    hh = line([(j-1)/br^(it-1)+bb/br^it  (j-1)/br^(it-1)+bb/br^it],...
                             [(i-1)/br^(it-1)      i/br^(it-1)]);
                    set(hh, 'LineWidth',lwidth, 'Color',[0 0 0])
                end
                matnew((i-1)*br+1:i*br,(j-1)*br+1:j*br) = rulmat;
            end
        end
    end
    matold = matnew;
end

axis([0 1 0 1]);
set(gca,'Visible','off','Position',[0 0 1 1]);
set(gcf, 'NumberTitle','off','Name','Deterministic Fractal as Line','pos',[200 100 500 500]);
```

APPENDIX II B

```
% Random Fractal as Line
% Homogeneous Random Fractal
% rfln(maxit,b,pb)
% output : [Figure]
% maxit = maximum iteration number
% b    = scale factor
% pb   = probability (cells to be taken out)

% by Kim, Jung-Woo (2005)
% modified by Ankur Roy (2005)

function [] = rfln(maxit,b,pb,lwidth)

if maxit ~= abs(fix(maxit)) | b ~= abs(fix(b)) | pb ~= abs(fix(pb))
    disp('!!!! Wrong Input... Try it again... !!!!');
    return;
end

Figure;

matold = 0;
for it = 1:maxit
    [nrow ncol] = size(matold);
    matnew = ones(b^it,b^it);
    for i = 1:nrow
        for j = 1:ncol
            if matold(i,j) == 0
                for bb = 1:b-1
                    hh = line([(j-1)/b^(it-1)      j/b^(it-1)],...
                             [(i-1)/b^(it-1)+bb/b^it  (i-1)/b^(it-1)+bb/b^it]);
                    set(hh, 'LineWidth',lwidth, 'Color',[0 0 0])
                    hh = line([(j-1)/b^(it-1)+bb/b^it  (j-1)/b^(it-1)+bb/b^it],...
                             [(i-1)/b^(it-1)      i/b^(it-1)]);
                    set(hh, 'LineWidth',lwidth, 'Color',[0 0 0])
                end
                odr = zeros(b);
                rnd = randperm(b^2);
                for k = 1:b^2
                    if rnd(k) <= pb
                        odr(k) = 1;
                    else
                        odr(k) = 0;
                    end
                end
                matnew((i-1)*b+1:i*b,(j-1)*b+1:j*b) = odr;
            end
        end
    end
    matold = matnew;
end
```

```
axis([0 1 0 1]);  
set(gca,'Visible','off','Position',[0 0 1 1]);  
set(gcf, 'NumberTitle','off','Name','Random Fractal as Line','pos',[200 100 500 500]);
```

APPENDIX II C

```
% Lacunarity (2-Dimension)
% lacu2d(mat,wind,ps)
% OUTPUT lacunarity
% INPUT mat : original matrix
%      wind : unit window to compute lacunarity
%      ps : pore or solid (pore = 0; solid = 1)
% by Kim, Jung-Woo (2005)
% modified by Ankur Roy (2005)

function [] = lacu2d(wind,ps);
A= imread('b4n7i3rand.bmp');

[nrow ncol] = size(A);

imax = nrow-wind+1;
jmax = ncol-wind+1;
tot = imax*jmax;

s = [];
for i = 1:imax
    for j = 1:jmax
        s = [s, length(find(A(i:i+wind-1,j:j+wind-1) == ps))];
    end
end

np = [];
mom1 = 0;
mom2 = 0;
for k = 0:wind^2
    n = length(find(s==k));
    np = [np; [k n n/tot]];
    mom1 = mom1 + np(k+1,1)*np(k+1,3);
    mom2 = mom2 + np(k+1,1)^2*np(k+1,3);
end

lac = mom2/(mom1^2)
```

APPENDIX II D

```
% my second program
% to find the porosity, mean and variance of a matrix
% by Ankur Roy (Nov, 2005)
```

```
function [] = porosity(param);
mat=imread('bartong_72dpi.bmp');
[br bc] = size(mat);
zero=0;
one=0;
for i=1:br
for j=1:bc
    if mat(i,j)==param
        zero=zero+1;
    else
        one=one+1;
    end
end
end
por=zero/(zero+one);
if param==0
    mean=one/(zero+one)
else
    mean=zero/(zero+one)
end
porosity = por*100
var = 0;
for i=1:br
for j=1:bc
    var=var+(mat(i,j)-mean)^2;
end
end
variance=var/(br*bc-1)
```

APPENDIX II E: TABLES

Table 2.1 Fracture porosities and lacunarities, $L(31)$ and $L(450)$, of synthetic fractal-fracture patterns with $D = 1.585$

model	$L(31)$	$L(450)$	% porosity
b2n1i4_det	1.8755	1.0087	5.146
b2n1i4_ran	1.8457	1.0013	5.144
b4n7i2_det	1.9287	1.0103	9.463
b4n7i2_ran	1.7903	1.0014	9.451

Table 2.2 Odling's (1997) maps: scales, *proxy* r_{min} (in meters), fractal dimension D_b , fracture porosity and lacunarities L_{upper} , $L(10)$ and $L(500)$

map no	area	scale	<i>proxy</i> r_{min} (m)	D_b	% porosity	$L(10)$	$L(500)$
1	18m x 18m	1:102	0.35	1.80 ± 0.05	5.73	2.4226	1.0072
2	55m x 55m	1:313	0.81	1.82 ± 0.04	7.85	2.0815	1.0071
3	90m x 90m	1:511	1.33	1.82 ± 0.05	8.50	1.9319	1.0031
4	90m x 90m	1:511	1.33	1.81 ± 0.05	7.95	2.0234	1.0209
5	180m x 180m	1:1023	2.4	1.82 ± 0.04	7.93	1.9363	1.0146
6	360m x 360m	1:2045	3.62	1.84 ± 0.04	10.09	1.6414	1.0063
7	720m x 720m	1:4091	7.25	1.84 ± 0.04	9.84	1.6078	1.0037

APPENDIX II F: FIGURES

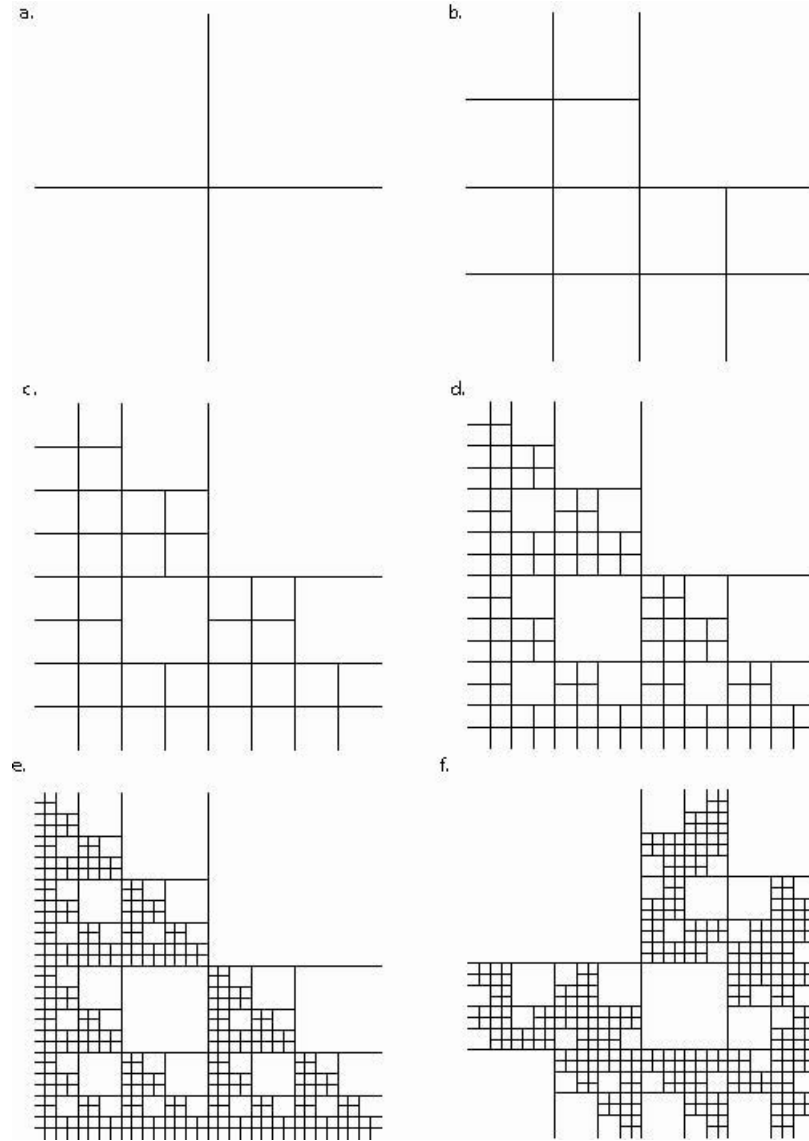


Figure 2.1 Construction of the deterministic fractal-fracture model b2n1_det: (a) basic template $i = 0$ with two fractures of length 1, (b) $i = 1$: addition of fractures of length $1/2$, (c) $i = 2$: addition of fractures of length $1/4$, (d) $i = 3$: addition of fractures of length $1/8$, (e) $i = 4$ (b2n1i4_det): addition of fractures of length $1/16$, (f) randomized version of (e): (b2n1i4_ran)

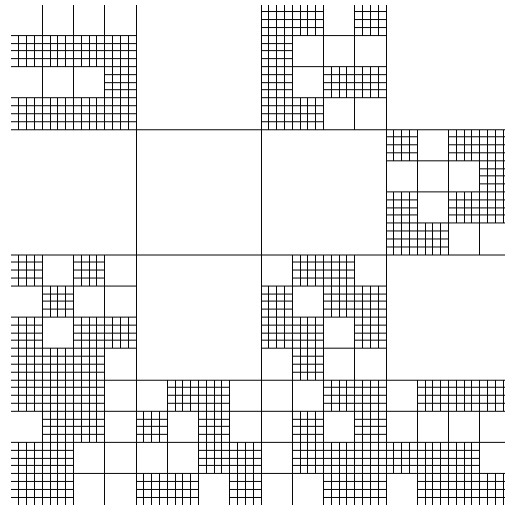
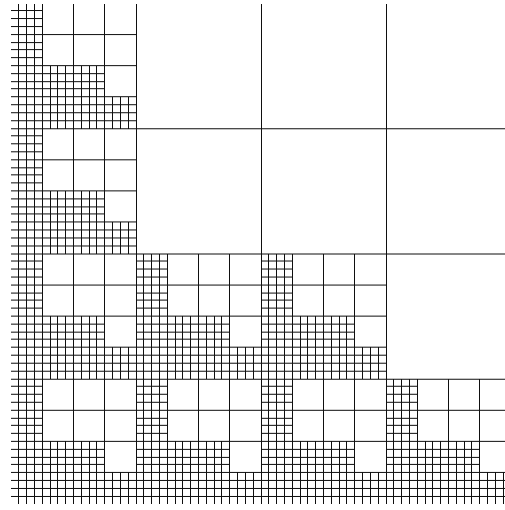


Figure 2.2 Deterministic (a) and randomized (b) fractal-fracture patterns (b4n7i2_det and b4n7i2_ran, respectively)

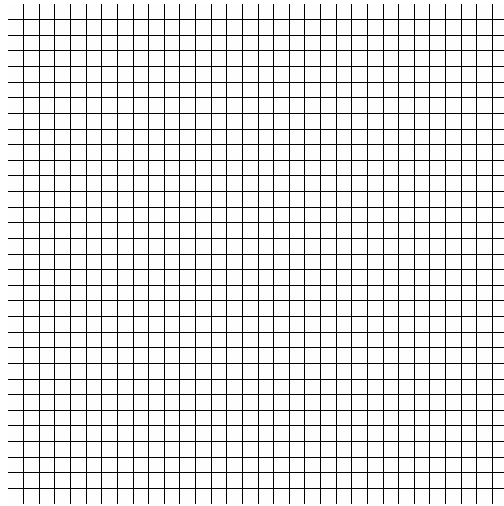


Figure 2.3 Translationally invariant set: simple 32 X 32 grid (non-fractal)

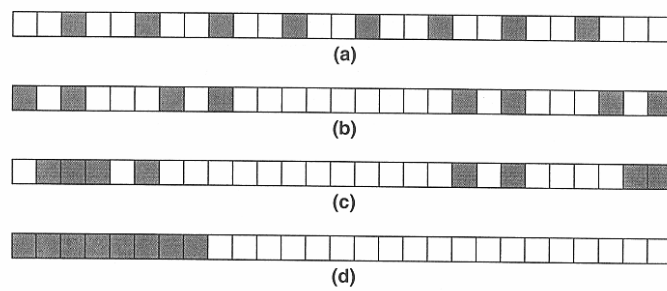


Figure 2.4 Linear patterns showing same number of filled units but differing in spatial distribution (from Turcotte, 1997)

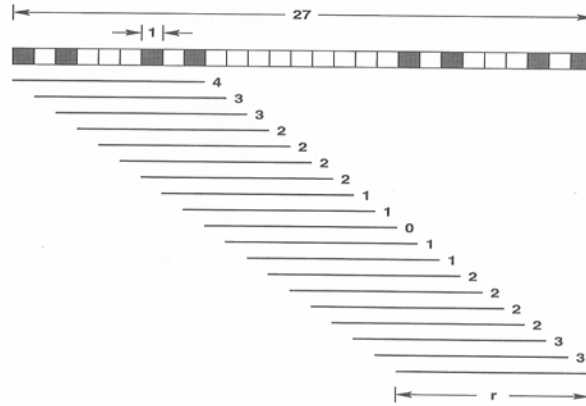


Figure 2.5 Gliding window algorithm showing distribution of $n(s, r)$ for $r=9$ (from Turcotte, 1997)

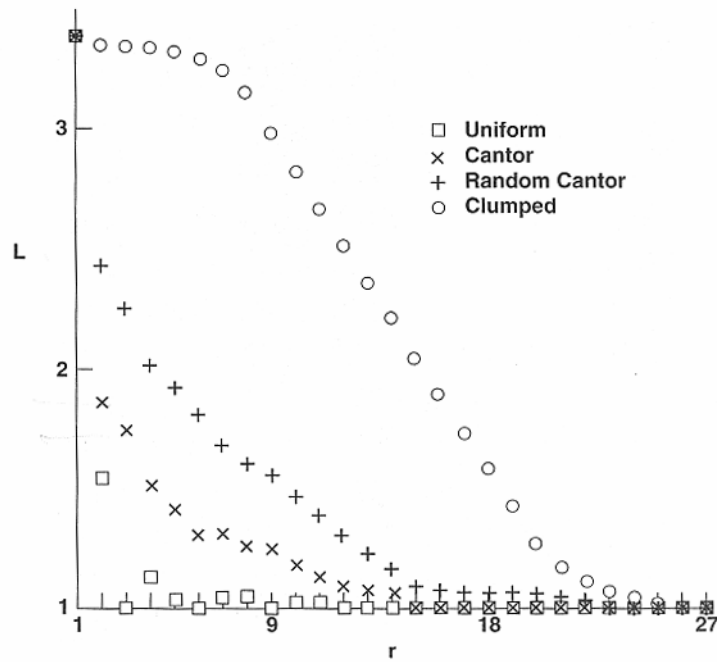


Figure 2.6 Lacunarity analyses of the distributions shown in 2.4 (from Turcotte, 1997)

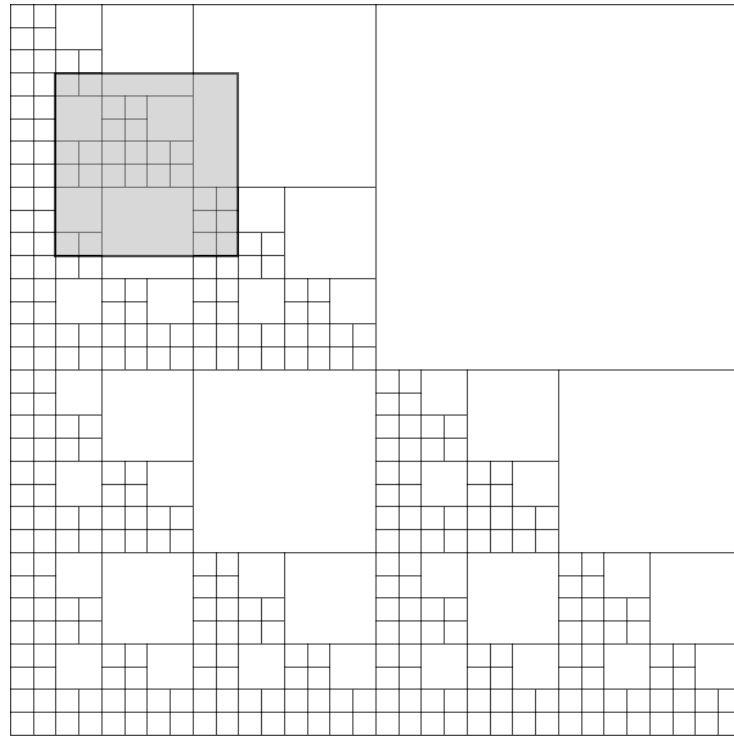


Figure 2.7 Gliding-window in a typical fractal-fracture pattern: b2n1i4_det

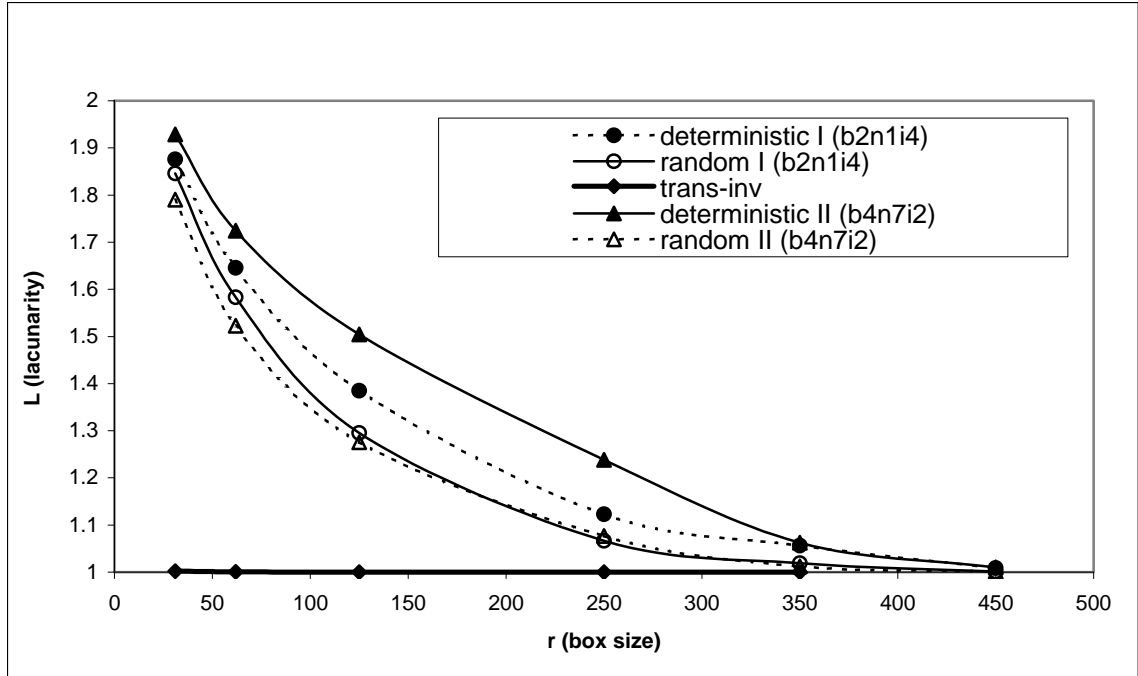


Figure 2.8 $L(r)$ vs. r plots for patterns b2n1i4_det, b2n1i4_ran, b4n7i2_det, b4n7i2_ran and trans-inv

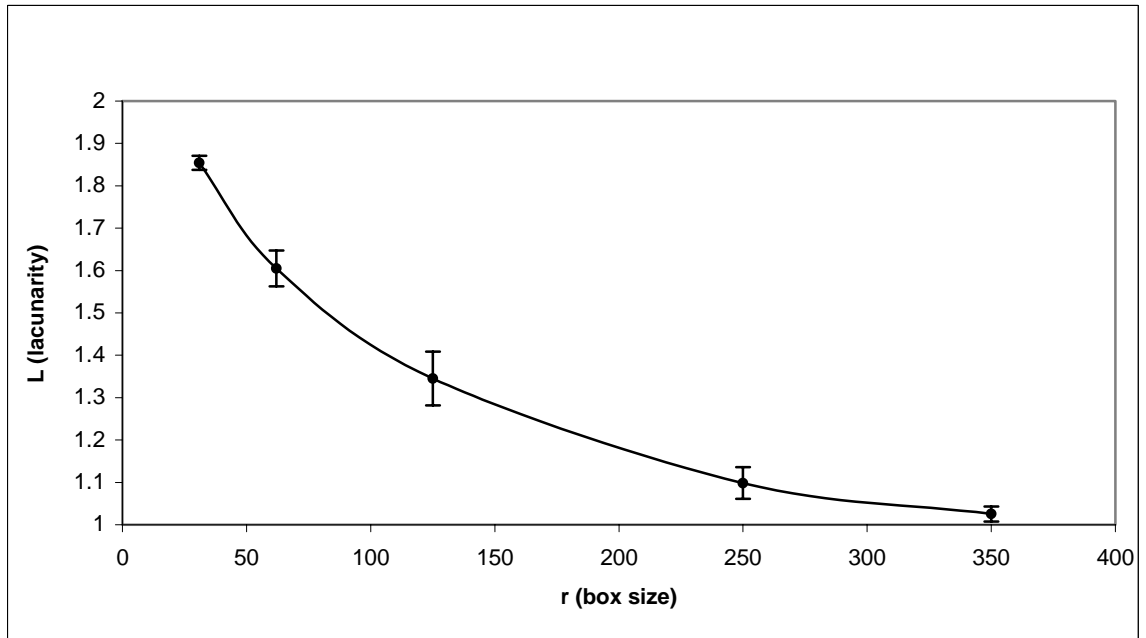


Figure 2.9 Mean and standard deviations of $L(r)$ vs. r plots for 10 randomized versions of b2n1i4_ran

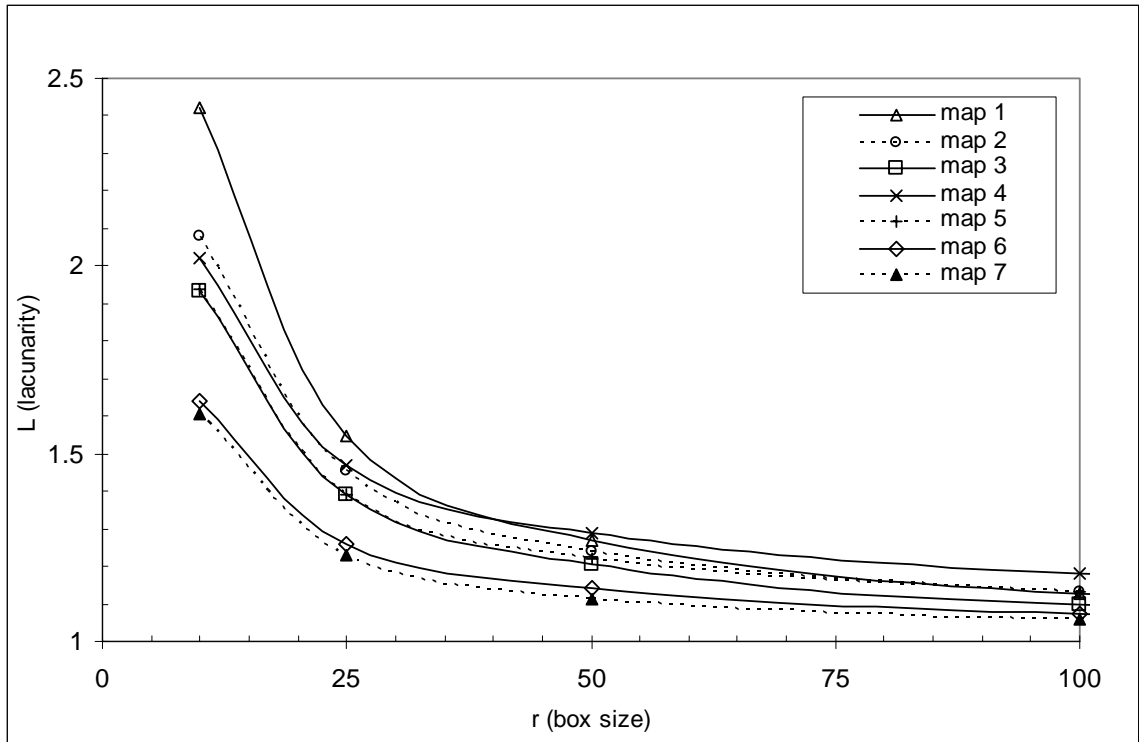


Figure 2.10 $L(r)$ vs. r curves for Odling's maps 1-7

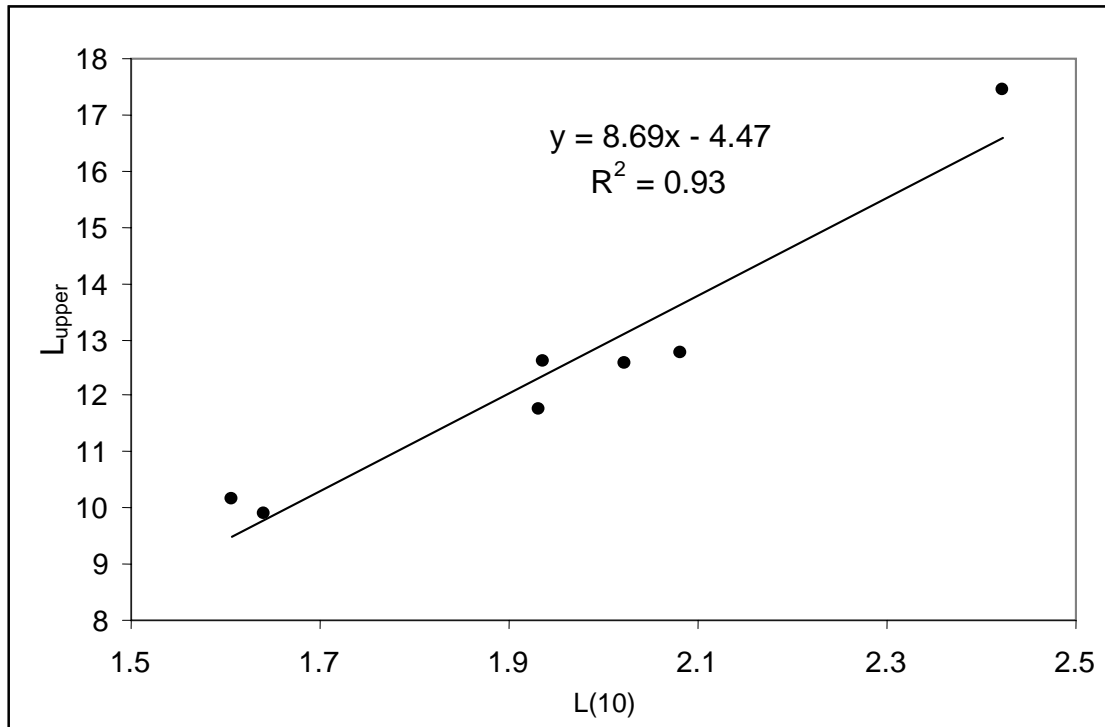
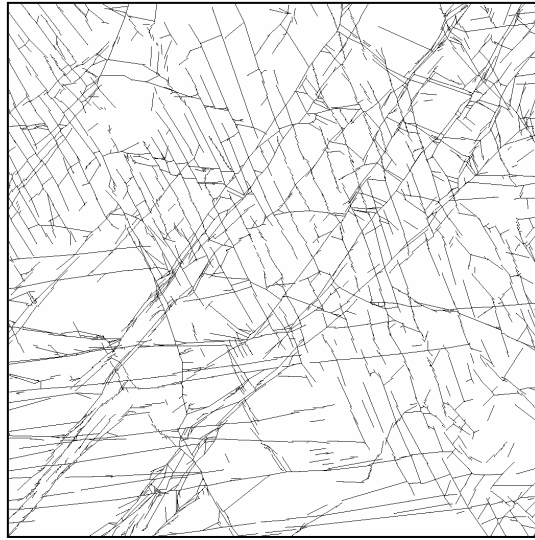


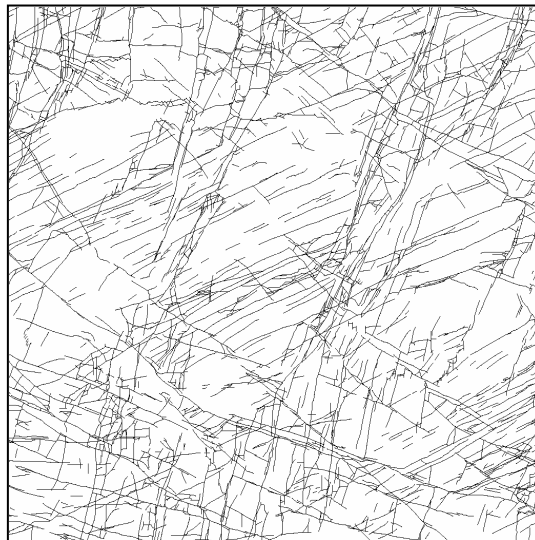
Figure 2.11 L_{upper} ($=l/\phi$) vs. $L(10)$ for Odling's (1997) maps 1-7

GENERAL APPENDICES

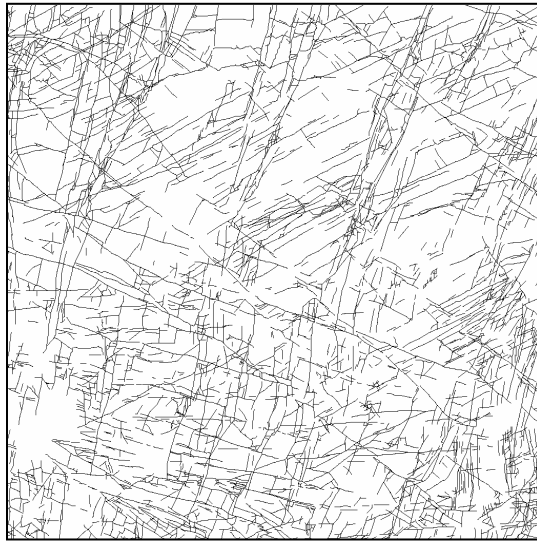
APPENDIX A: ODLING'S MAPS



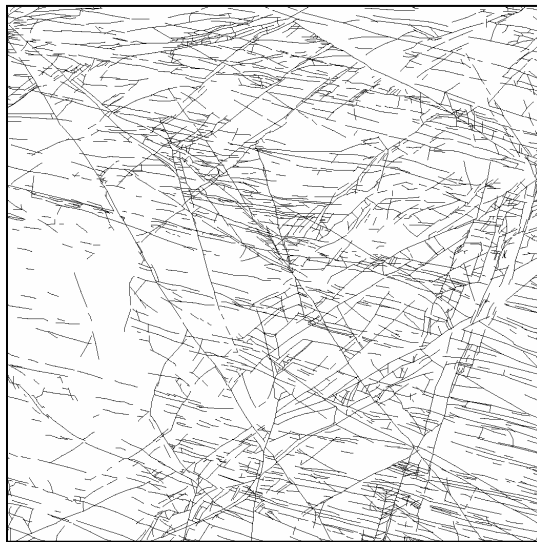
Map 1: horn_ya



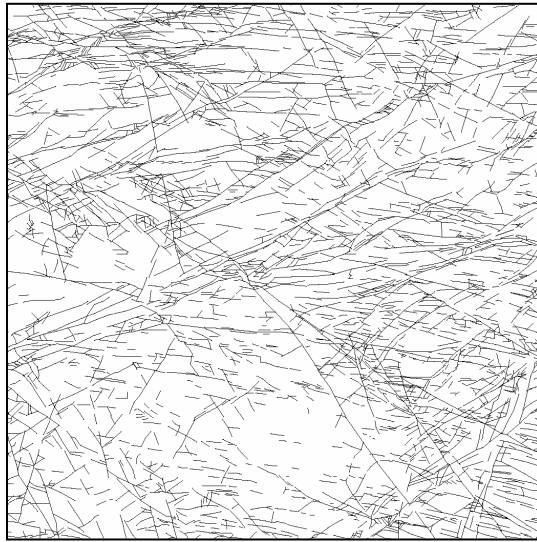
Map 2: horn_yb



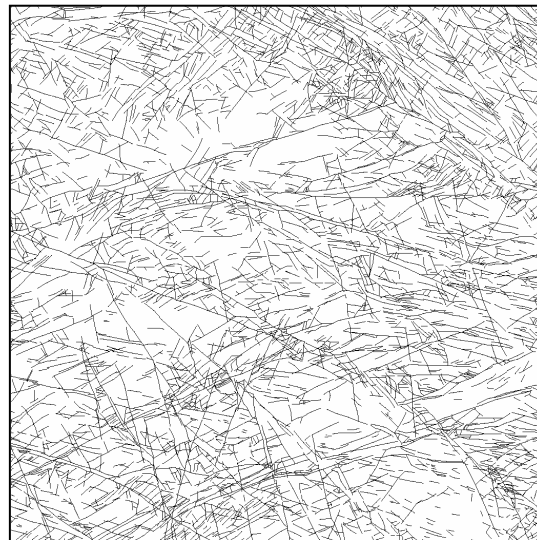
Map 3: horn_yc



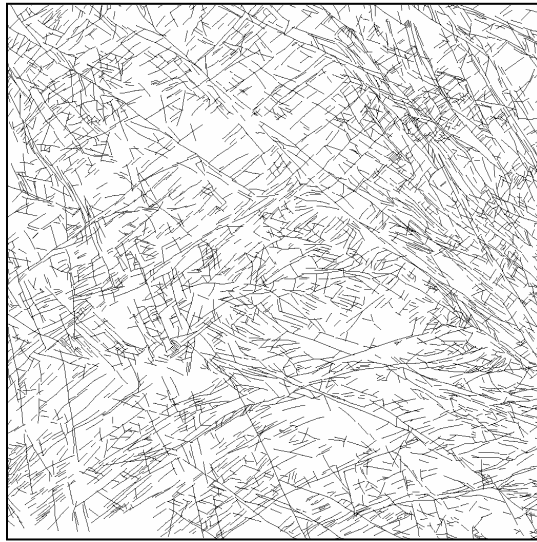
Map 4: horn_sa



Map 5: horn_sb



Map 6: horn_sc



Map 7: horn_sd

APPENDIX B: BARTON'S MAPS



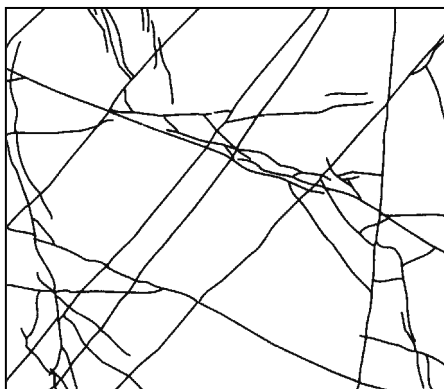
Map a: uncropped



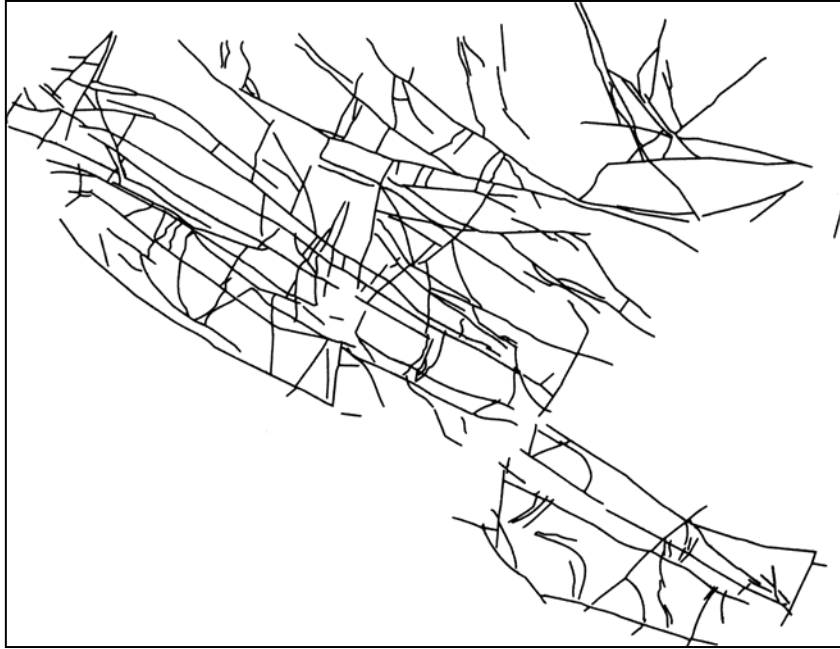
Map a: cropped



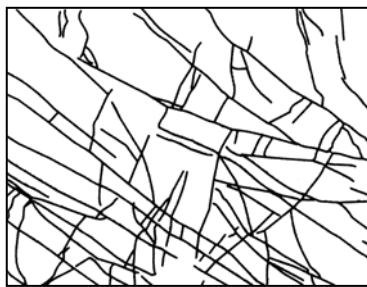
Map b: uncropped



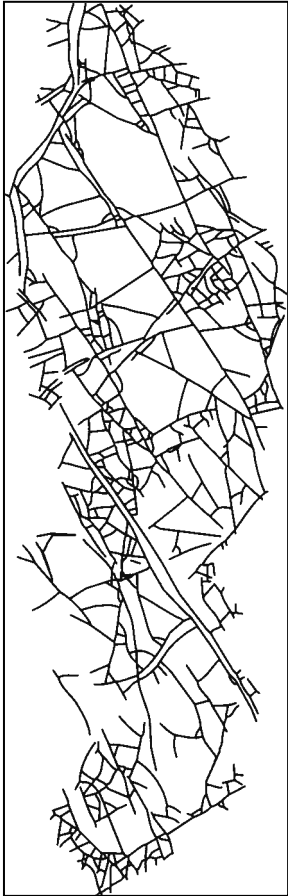
Map b: cropped



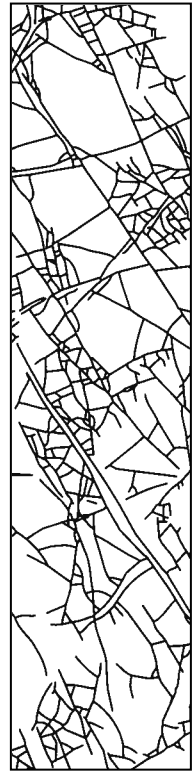
Map c: uncropped



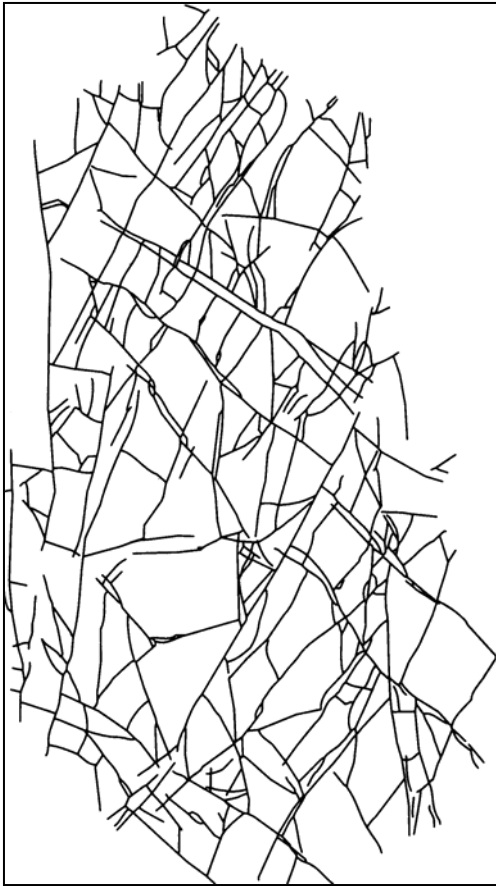
Map c: cropped



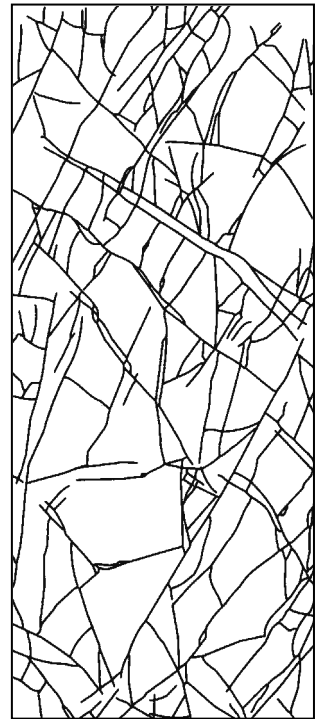
Map d: uncropped



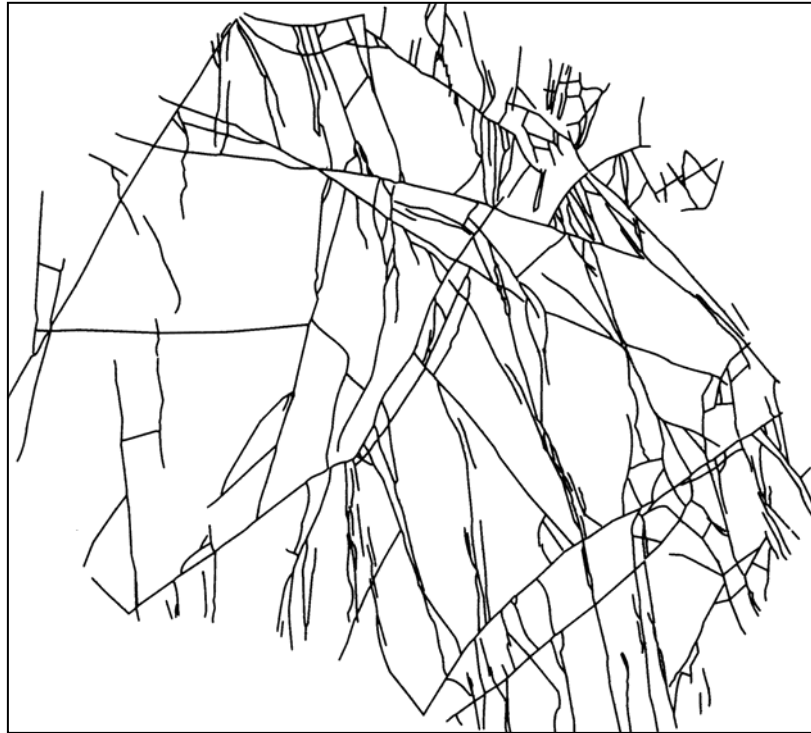
Map d: cropped



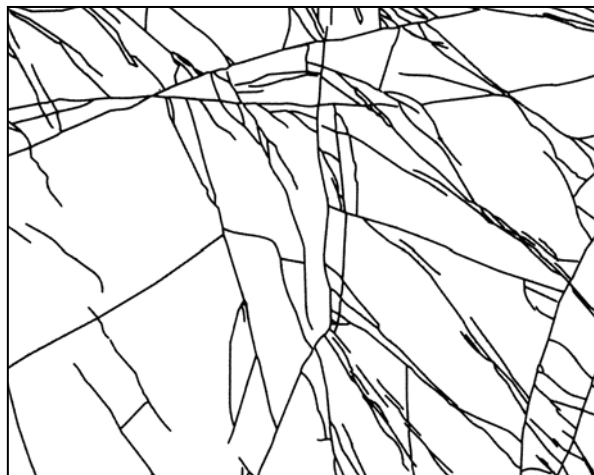
Map e: uncropped



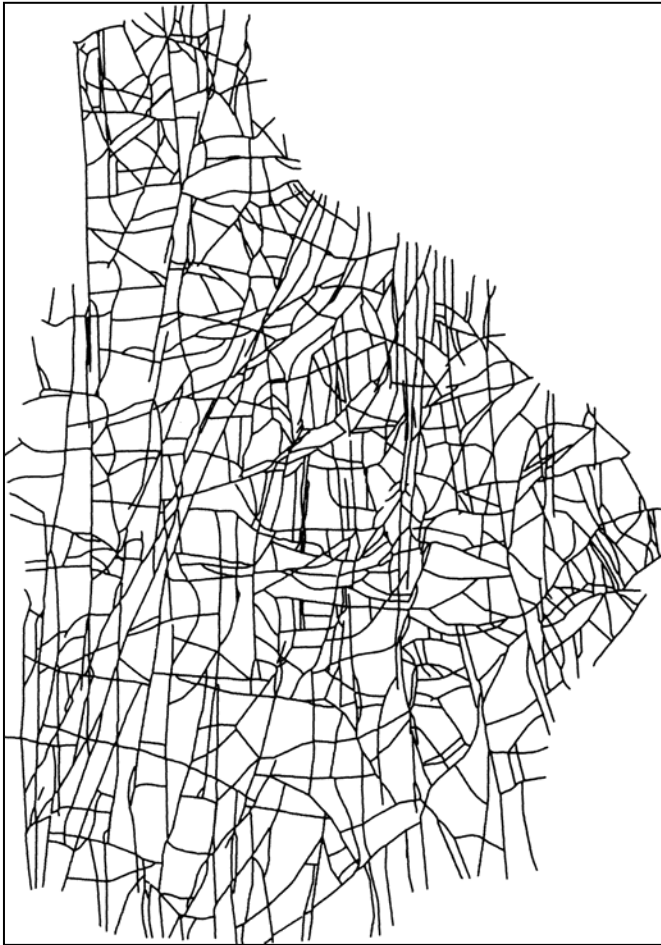
Map e: cropped



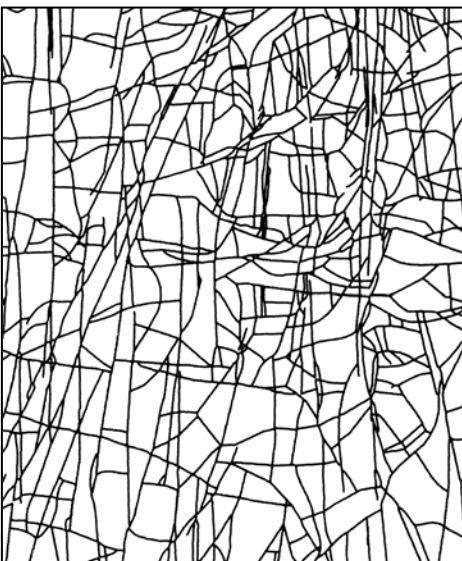
Map f: uncropped



Map f: cropped



Map g: uncropped



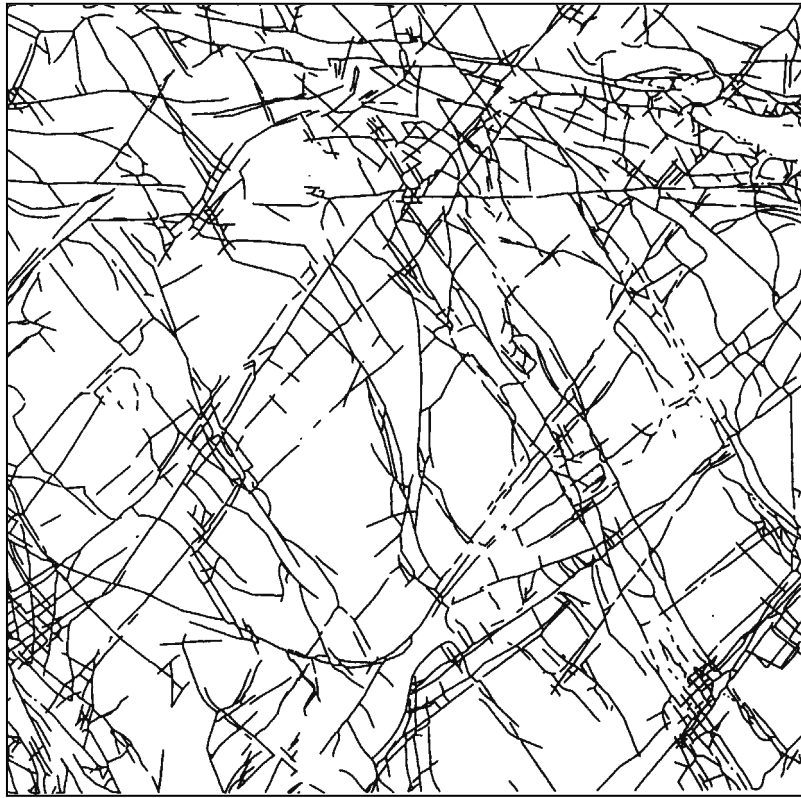
Map g: cropped



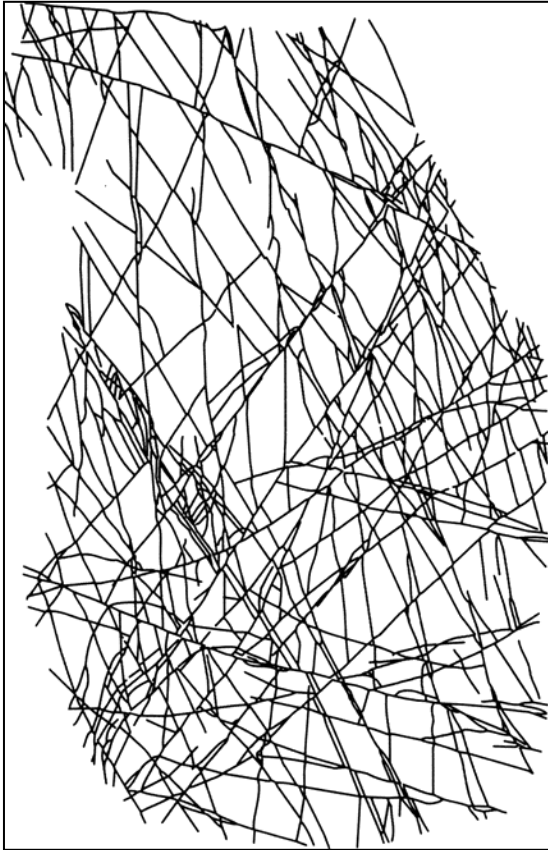
Map h: uncropped



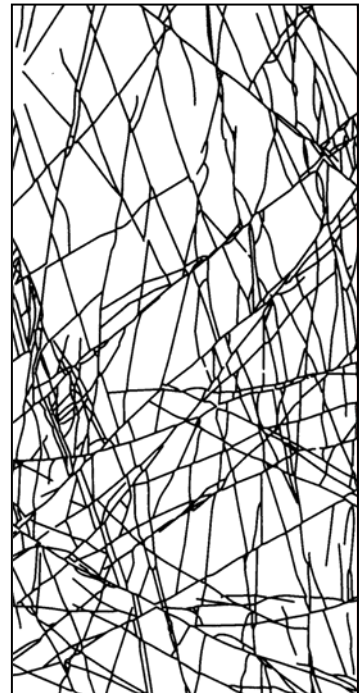
Map h: cropped



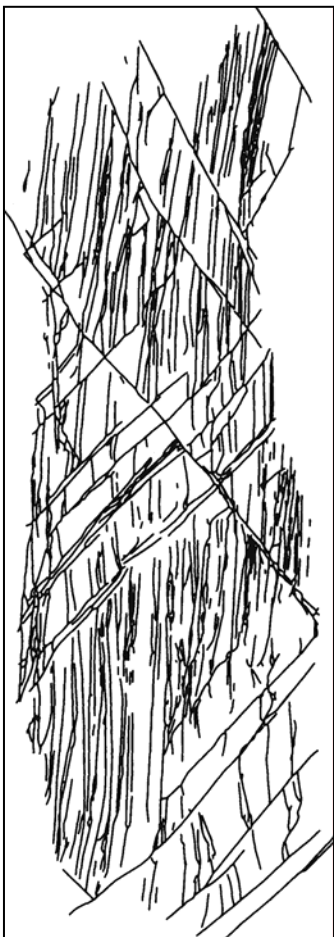
Map i: uncropped



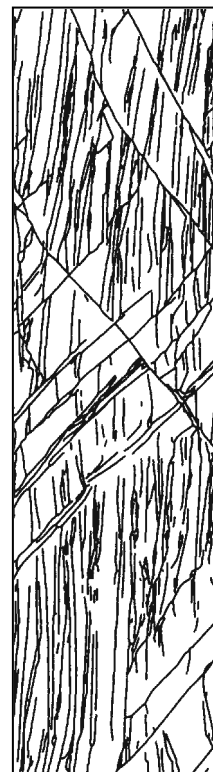
Map j: uncropped



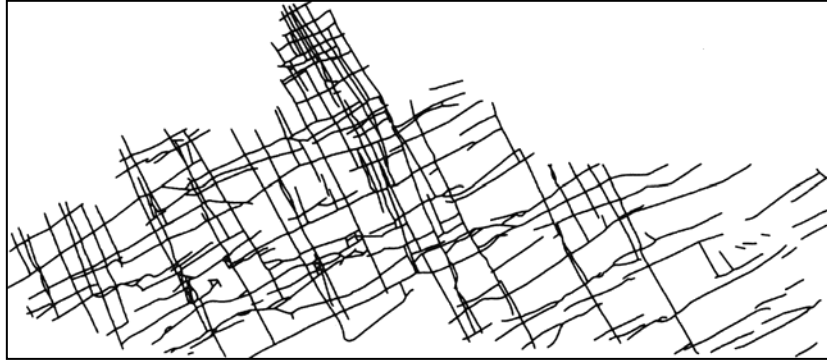
Map j: cropped



Map k: uncropped



Map k: cropped



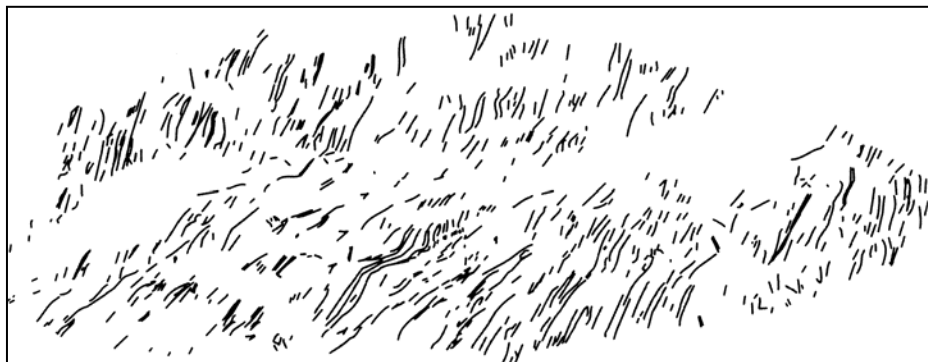
Map 1: uncropped



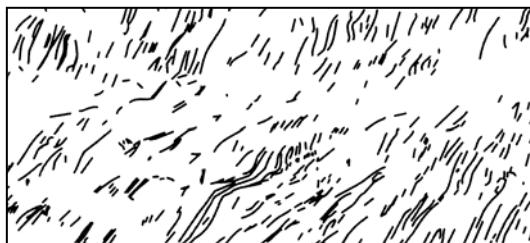
Map 1: cropped



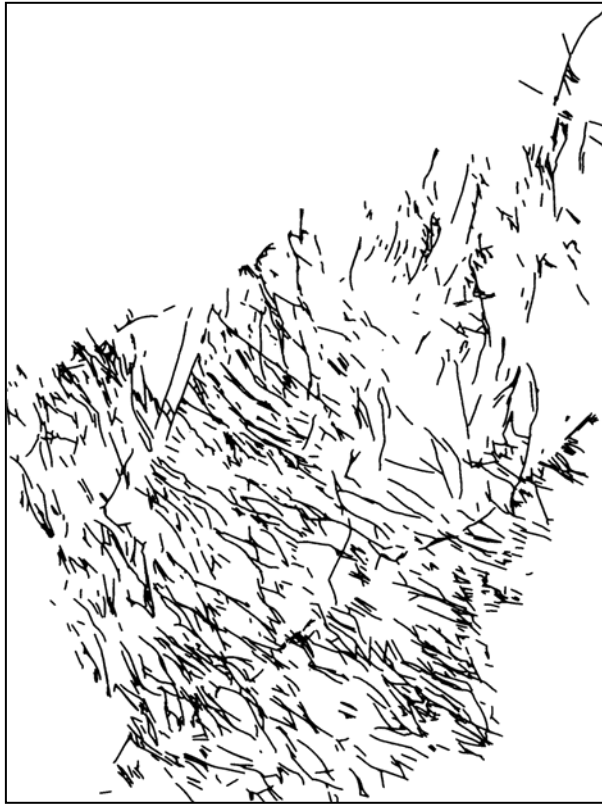
Map m: uncropped



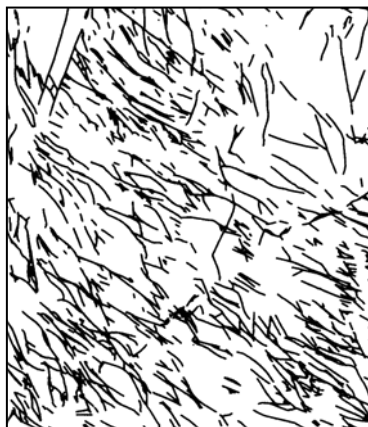
Map n: uncropped



Map n: cropped



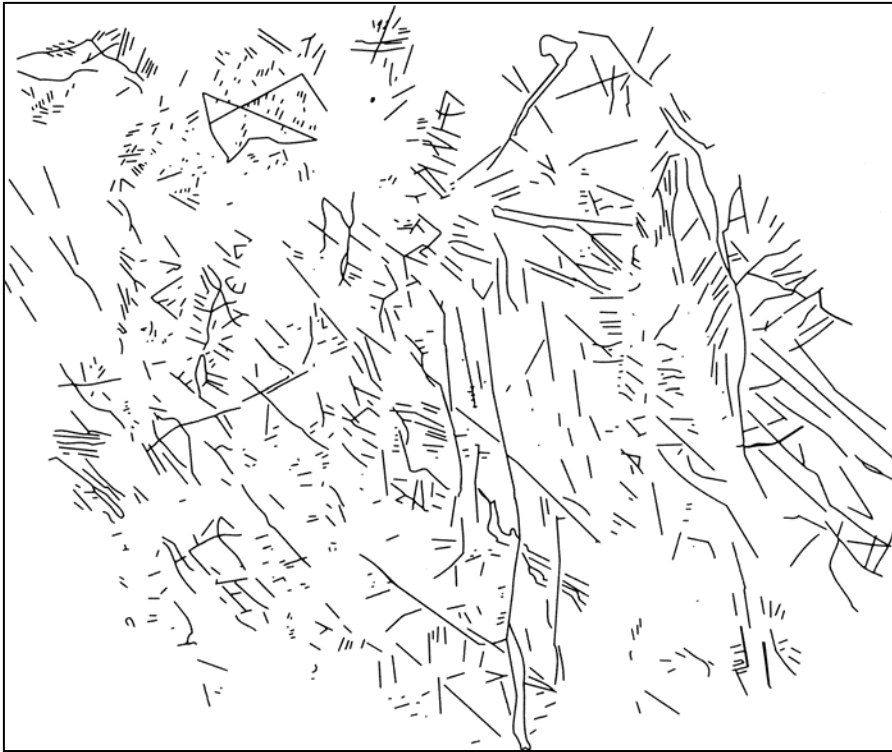
Map o: uncropped



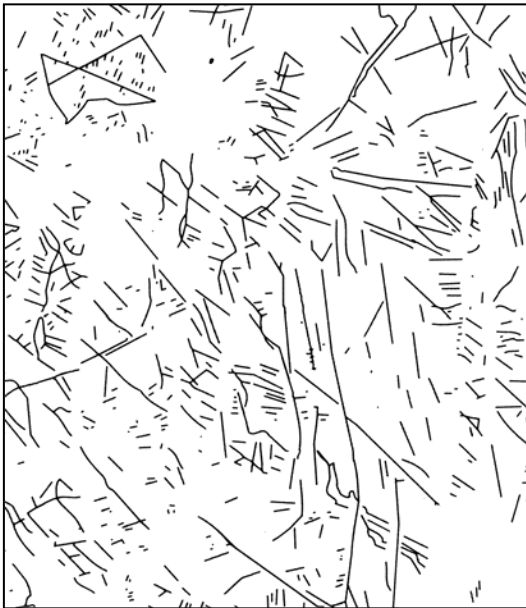
Map o: cropped



Map p: uncropped



Map q:
uncropped



Map q: cropped

VITA

Ankur Roy was born on September 12, 1977, in Calcutta, India. His childhood interest in unraveling the myriad mysteries of nature eventually led him to pursue an honors curriculum in Geology at the prestigious Presidency College in Calcutta. After graduating with a BSc degree in 2000, he completed a masters program at the Indian Institute of Technology, Kharagpur (India), where he focused mainly on sedimentology and worked on an MSc thesis titled “Ripple Characteristics of the Intertidal regions of Digha and Chandipur.” Ankur’s interest in fundamental research in geological sciences brought him overseas where he has sought a thesis based MS in the Department of Earth and Planetary Sciences at the University of Tennessee, Knoxville. Here, his interest in the world of numbers and diverse areas of science led him to take the course on Fractal Models in Earth Sciences offered in this department by Dr. Ed Perfect. This was a turning point in his career, helping him to choose an advisor and define an MS project. His keen interest in structural geology as an undergrad at Presidency College and a general knack for mathematical applications led him to the present course of his studies, where he essentially seeks to address issues related to the scaling properties of fracture networks. Ankur will soon matriculate at the Jackson School of Geosciences at the University of Texas, Austin, where he plans to work in the Fracture Research Program for his doctoral studies.